Table 4 Number of the sick/wounded persons classified by the participating teams in 2003

Participating team	Number of games*	Number of spectators*	Number of spectators per game	Number of sick/wounded persons	Number of sick/wounded persons per game	Number of sick/wounded persons per 10.000 spectators	Relative risk level per game**	Relative risk level per 10.000 spectators**
Hanshin Tigers	12	482,000	40,167	99	7.6	2.05	4.47	2.13
Chunichi Dragons	10	154,000	15,400	19	1.9	1.23	1.12	1.28
Yomiuri Giants	14	493,000	35,214	75	5.0	1.52	2.94	1.58
Hiroshima Toyo Carp	12	208,000	17,333	20	1.7	0.96	1.00	1.00
Yokohama Bay Stars	11	190,000	17,273	26	2.4	1.36	1.41	1.42
Exhibition game	6	55,000	9,167	8	1.3	1.45	0.76	1.51
Total	65	1,582,000		247	3.7	1.56		

* Excluding the called-off games
** The risk level for the game relative to that for a competitor with the lowest incidence of sickness and injury is set as 1.
Number of the sick / wounded persons classified by the participating teams was analyzed from "Report of Aid" in 2003.

risk (*i.e.* incidence of visits to the first-aid station) per spectator was 2.13 times as high as that for the participating team with the lowest incidence, and the risk per game was 4.47 times as high as that for the team with the lowest incidence. These results suggest that the extent of medical preparedness needed at the first-aid station in the stadium varies according to the participating teams.

The survey of "Report of Accidents" revealed that intrinsic cardiopulmonary arrest (CPA) occurred in one spectator during the 8-year study period. By-stander cardiopulmonary resuscitation (CPR) was not employed and there was no record of the initial heart rhythm. Thus, even ballparks should be equipped with an AED to rescue spectators who might suffer CPA.[15] Recently, the Full Cast Stadium at Sendai (the home ground of a new ball club) was equipped with 12 AEDs.

In summary, the results of the present study show that there is a constant risk to even spectators at ballparks, although these data have been collected from only one stadium. Medical care is needed even for spectators of professional baseball games and the on-site first-aid station at the stadium may reduce the need for clinics/hospitals visits referral. It is considered that meticulous maintenance of records of the sick/wounded at public facilities would allow a reasonable analysis of the demand for medical preparedness at any particular facility, as well as planning of reasonable medical care posts at other similar facilities.

Acknowledgement

We wish to thank Mr. Takayuki Okitsu, the former manager of Meiji Jingu Stadium, and Mr. Kazunari Wakatsuki, the person-in-charge of the safety of the stadium, who kindly shared with us valuable data from the Meiji Jingu Baseball Stadium, Meiji Jingu Gaien. We would also like to express our gratitude to the on-site physicians and nurses at the stadium.

References

1. Milsten AM, Maguire BJ, Bissell RA, Seaman KG: Mass-gathering medical care: a review of the literature. Prehosp Disast Med 2002; 17: 151–162
2. Roberts DM, Blackwell TH, Marx JA: Emergency medical care for spectators attending national football league games. Prehosp Emerg Care 1997; 1: 149–155
3. Howe WB. The team physician. Prim Care 1991; 18: 763–775
4. Ishii N, Nakayama S, Nakamura M, Ohmori Y, Matsuyama S, Maeda Y, Nakao H, Okada N, Takahashi A: Review on emergency medical management for mass gathering disaster in the 2002 FIFA World Cup: in the case of Kobe venue. J J Disast Med 2004; 8: 238–248
5. Katsumi A, Morimura N, Koido Y, Sugimoto K, Fuse A, Asai Y, Ishii N, Ishihara T, Sugiyama M, Yoshioka T, Fujii C, Henmi H, Yamamoto Y: A questionnaire survey on establishment of mass casualty disaster management system at the 2002 FIFA World Cup Korea/Japan. J J Disast Med 2004; 9: 45–51(in Japanese with English abstract)
6. Thompson JM, Savoia G, Powell G, Challis EB, Law P: Level of medical care required for mass gatherings: the XV Winter Olympic Games in Calgary, Canada. Ann Emerg Med 1991; 20: 385–390
7. Pons PT, Holland B, Alfrey E, Markovchick V, Rosen P, Dinerman N: An advanced emergency medical care system at national football league games. Ann Emerg Med 1980; 9: 203–206
8. Kurakake S, Okamura N, Kumae T, Ohshita Y, Totsuka M, Umeda T, Nakaji S, Sugawara K: Kakino koukou-yakyu kansensya no hakkan-ryo to suibun-sessyu. J Phys Fit Nutr Immunol 2000; 10: 138–140 (in Japanese)
9. Burns LS, Ellison PA: First aid and emergency care at a major-league baseball stadium. J Emerg Nurs 1992; 18: 329–334
10. Morimura N, Katsumi A, Koido Y, Sugimoto K, Fuse A, Asai Y, Ishii N, Ishihara T, Sugiyama M, Yoshioka T, Fujii C, Henmi H, Yamamoto Y: Monitoring system for the information of emergency patients related to the 2002 FIFA World Cup games in Japan via Internet mailing list. J J Disast Med 2004; 8: 249–257

(in Japanese with English abstract)
11. Hewitt S, Jarrett L, Winter B: Emergency medicine at a large rock festival. J Accid Emerg Med 1996; 13: 26–27
12. Nicholls RL, Elliott BC, Miller K: Impact injuries in baseball: prevalence, aetiology and the role of equipment performance. Sports Med. 2004; 34: 17–25.
13. Kyle JM, Leaman J, Elkins G: Planning for scholastic cardiac emergencies: the reply project. W V Med J 1999. 95: 258–260
14. Grange JT, Baumann GW, Vaezazizi R: On-site physicians reduce ambulance transports at mass gatherings. Prehosp Emerg Care 2003; 7: 322–326
15. Crocco TJ, Sayre MR, Liu T, Davis SM, Cannon C, Potluri J: Mathematical determination of external defibrillators needed at mass gatherings. Prehosp Emerg Care 2004; 8: 292–297

Prostaglandin E_2 Induces Hypertrophic Changes and Suppresses α-Skeletal Actin Gene Expression in Rat Cardiomyocytes

Satoru Miyatake, MD,† Haruko Manabe-Kawaguchi, PhD,* Kikuko Watanabe, PhD,‡ Shingo Hori, MD, PhD,† Naoki Aikawa, MD, PhD, FACS,† and Keiichi Fukuda, MD, PhD, FACC**

Abstract: Prostaglandin E_2 (PGE_2) is a potent lipid mediator in a diverse range of biological processes. This study examined the hypertrophic effect of PGE_2 in primary cultured rat neonatal cardiomyocytes. PGE_2 increased total protein synthesis in a dose-dependent manner, as measured by [^{3}H]-phenylalanine uptake. PGE_2 increased the cell size and surface area and induced the reorganization of myofilaments. Phosphorylation of the p42/44 and p38 mitogen-activated protein kinases (MAPK) was also induced by PGE_2, and U0126 [a mitogen-activated extracellular signal regulated kinase kinase (MEK) 1/2 inhibitor] significantly inhibited the PGE_2-induced protein synthesis. Expression of the hypertrophic marker genes, atrial natriuretic peptide and brain natriuretic peptide, was increased by PGE_2, but expression of the α-skeletal actin gene was significantly attenuated. Transcripts for all 4 PGE_2 receptor subtypes (EP_1, EP_2, EP_3, and EP_4) were detected in the cardiomyocytes. AE3-208 (an EP_4-selective antagonist) significantly inhibited the α-skeletal actin gene suppression induced by PGE_2, whereas SC51322 (an EP_1-selective antagonist) did not. In conclusion, PGE_2 induced hypertrophic changes in cardiomyocytes and attenuated α-skeletal actin gene expression in part via EP_4.

Key Words: prostaglandin E_2, cardiac hypertrophy, α-skeletal actin

(*J Cardiovasc Pharmacol*™ 2007;50:548–554)

INTRODUCTION

Prostaglandin E_2 (PGE_2) is widely distributed in various organs and is involved in diverse biological processes such as induction of pain, fever, immunity, tumorigenesis, and inflammation.[1,2] PGE_2 also induces cell proliferation and morphological changes in various cell lines.[3,4] It acts via 4 receptor subtypes: EP_1, EP_2, EP_3, and EP_4. These receptors couple to G proteins and influence signaling in a variety of intracellular messenger pathways. EP_1 couples to G_q and increases the levels of intracellular Ca^{2+}. EP_2 and EP_4 couple to G_s and effect a rise in intracellular cyclic AMP concentration, whereas EP_3 couples to G_i and inhibits cyclic AMP production.[5] In ventricular myocytes, PGE_2 stimulates cyclic AMP production and increases protein synthesis, in part via EP_4.[6,7]

The biosynthesis of PGE_2 is mediated by 3 enzymatic reactions involving phospholipase A_2, cyclooxygenase, and prostaglandin E synthase (PGES). Three types of PGES have been cloned in mammals: membrane-associated PGES-1, membrane-associated PGES-2, and cytosolic PGES.[8–12] The heart expresses all of these PGESs,[12,13] suggesting that PGE_2 plays a pivotal role in modulating cardiac function.

To date, a number of growth factors and cytokines that induce cardiac hypertrophy have been isolated. In cardiomyocytes, these factors not only promote protein synthesis but also induce immediate early genes such as c-fos and hypertrophy marker genes, such as atrial natriuretic peptide (ANP) and brain natriuretic peptide (BNP).[14,15] α-skeletal actin is expressed during cardiac development and then downregulated after birth in mammals.[16] Its expression is activated by most cardiac hypertrophic stimuli, including angiotensin II, endothelin-1, phenylephrine,[17–20] and pressure overload,[21–23] and it has become a well-accepted marker of cardiac hypertrophy. However, several other stimuli, including cardiotrophin-1[24] and interleukin-1β (IL-1β),[25] induce distinct hypertrophic phenotypes in which α-skeletal actin expression is not activated. These findings indicate that cardiac hypertrophic factors activate diverse signal transduction pathways and have distinct effects on cardiomyocyte gene expression.

The aim of this study was to test the hypothesis that PGE_2 induces hypertrophic changes in cultured cardiomyocytes, and to investigate any associated changes in gene expression for ANP, BNP, and α-skeletal actin.

METHODS

Cell Culture

Primary cultures of cardiomyocytes were prepared from the ventricles of 1-day-old neonatal Wistar rats (Japan CLEA, Tokyo, Japan), as described previously.[26] The rats were anesthetized with diethyl ether during the procedure.

Received for publication February 22, 2007; accpeted June 20, 2007.

From the *Department of Regenerative Medicine and Advanced Cardiac Therapeutics, Keio University School of Medicine, Tokyo, Japan; †Department of Emergency and Critical Care Medicine, Keio University School of Medicine, Tokyo, Japan; and ‡Division of Life Sciences, Graduate School of Integrated Sciences and Arts, University of East Asia, Yamaguchi, Japan.

The authors state that they have no financial interest in the products mentioned within this article.

Reprints: Keiichi Fukuda, MD, PhD, FACC, Department of Regenerative Medicine and Advanced Cardiac Therapeutics, Keio University School of Medicine, 35 Shinanomachi, Shinjuku-ku, Tokyo 160-8582, Japan (e-mail: kfukuda@sc.itc.keio.ac.jp).

Differential adhesiveness was used to separate cardiomyocytes from other cell types. Cardiomyocyte-rich cultures were produced by seeding nonattached cells at a density of 5×10^5 cells/cm^2 on gelatin-coated dishes. The cells were incubated in serum-free medium for 24 hours and then stimulated with PGE_2 (Cayman Chemical, Ann Arbor, MI). All experimental procedures and protocols were approved by the Animal Care and Use Committees of the Keio University and conformed to the National Institutes of Health Guide for the Care and Use of Laboratory Animals.

Incorporation of [^{3}H]-Phenylalanine Into Rat Neonatal Cardiomyocytes

Cardiomyocytes were cultured in gelatin-coated 24-well plates, serum depleted for 24 hours, and incubated with various concentrations of PGE_2 (1, 10, 100, 250, or 500 μM) for 24 hours. [^{3}H]-phenylalanine was added at the same time as PGE_2. In some experiments, cardiomyocytes were pretreated with U0126 [10 μM: a mitogen-activated extracellular signal regulated kinase kinase (MEK) 1/2 inhibitor (BIOMOL, Plymouth Meeting, PA)] or SB203580 [10 μM: a p38 MAPK inhibitor (BIOMOL)] for 1 hour, and then PGE_2 (10 μM) was added for another 24 hours. After washing the wells, [^{3}H]-phenylalanine uptake was measured with a liquid scintillation counter, as described previously.[26]

Immunofluorescence Microscopy and Measurement of Cell Size

After 24 hours of serum depletion, cardiomyocytes were stimulated with PGE_2 (250 μM) for 48 hours on glass coverslips. The cells were then permeabilized in 4% paraformaldehyde. After fixation, the cells were stained with antisarcomeric myosin antibodies (MF-20), as described previously.[26] Immunofluorescence images of stained sarcomeric myosin were obtained by confocal laser scanning microscopy (LSM-510 Meta; Carl Zeiss, Jena, Germany). The cell areas and perimeters were measured using NIH Image software.

Western Blot Analysis

After 24 hours of serum depletion, cardiomyocytes were stimulated with PGE_2 at a concentration of 250 μM for 2, 5, 15, 30, or 60 minutes. The cells were then washed with phosphate-buffered saline and lysed as described previously.[26] The lysate protein composition was analyzed by SDS-PAGE. Fractionated proteins were electrotransferred from the gels to reinforced nitrocellulose membranes, which were incubated with mouse monoclonal antibody against the phosphorylated forms (Thr202/Tyr203) of p42/44 mitogen-activated protein kinase (MAPK) and with rabbit polyclonal antibody against the phosphorylated form (Thr180/Tyr182) of p38 MAPK (Cell Signaling Technology, Danvers, MA). The membranes were then incubated with peroxidase-conjugated horse anti-mouse IgG or goat anti-rabbit IgG (Cell Signaling Technology). Signals were visualized with Super Signal West Pico Chemiluminescent Substrate (Pierce Biotechnology, Rockford, IL). After the detection, the membranes were incubated with Stripping Buffer (Pierce Biotechnology) and washed with Tirs-buffered saline Tween-20 and then incubated with rabbit polyclonal antibodies against the p42/44 MAPK and p38

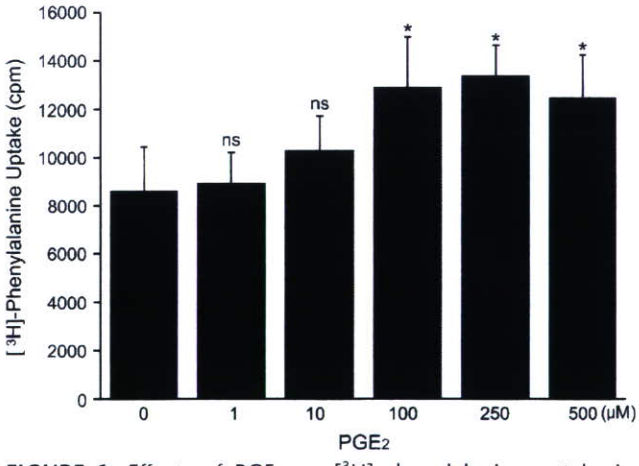

FIGURE 1. Effects of PGE_2 on [^{3}H]-phenylalanine uptake in cardiomyocytes. Cardiomyocytes were incubated with PGE_2 at concentrations ranging from 1.0 to 500 μM for 24 hours. The measurement of [^{3}H]-phenylalanine uptake is indicated. Each column represents the mean ± SD of 4 separate experiments. *$P < 0.05$ versus control; ns, not significant.

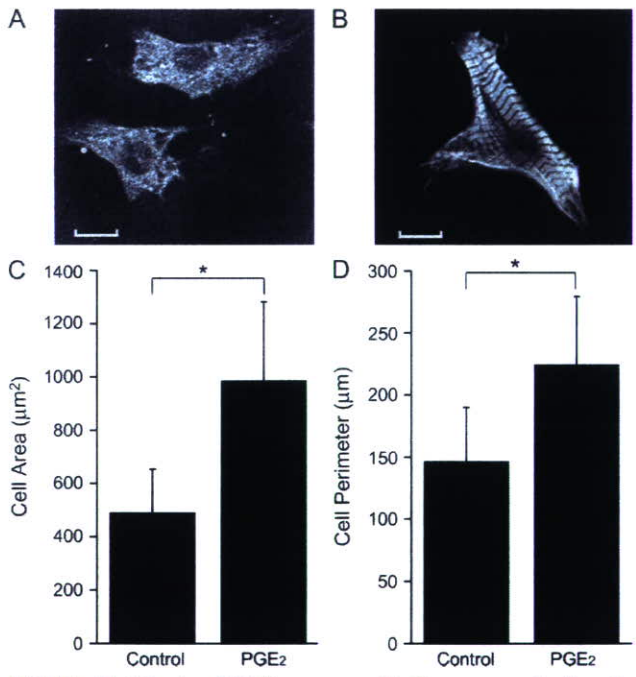

FIGURE 2. Effects of PGE_2 on myofibrillar reorganization in cardiomyocytes. (A, B) Representative immunofluorescence images of cardiomyocytes stained with antisarcomeric myosin antibody. The white bar represents 10 μm. (A) Control cardiomyocytes cultured without serum for 48 hours. (B) Cardiomyocyte exposed to PGE_2 for 48 hours. PGE_2 caused an increase in cardiomyocyte size, as shown by measurement of cell area (C) and cell perimeter (D). Results are the mean ± SD of 100 cells. *$P < 0.05$ versus control.

MAPK (Santa Cruz Biotechnology, Santa Cruz, CA). The densities of the phosphorylated forms of the p42/44 MAPK and p38 MAPK signals were quantified using NIH Image software.

RNA Extraction and Northern Blot Analysis

Total RNA was extracted using TRIzol Reagent (Invitrogen, Carlsbad, CA) from cardiomyocytes incubated with or without PGE_2 (250 μM). Total RNA (20 μg) was separated on a 1% MOPS/formaldehyde-agarose gel and blotted onto a nylon membrane. cDNA fragments for ANP, BNP, the α-skeletal actin 3′-untranslated region, and glyceraldehyde-3-phosphate dehydrogenase (GAPDH) were obtained by reverse transcription-polymerase chain reaction (RT-PCR) from the rat cardiomyocytes as described previously.[27] These cDNAs were labeled with [^{32}P]-dCTP (Amersham Biosciences, Piscataway, NJ) by the random priming technique and used as probes for hybridization. After transfer, the blots were immersed in Rapid-hyb buffer (Amersham Biosciences), and hybridization was performed. The blots were washed and exposed to X-ray films. The density of each blot was quantified using NIH Image software.

RT-PCR for Rat EP Receptors

Total RNA was extracted from cultured cardiomyocytes as described above. The RNA samples were treated with DNase I (Invitrogen), and cDNA was then synthesized by reverse transcription of the total RNA using oligo-dT primers (Invitrogen). To detect the 4 receptor subtypes (EP_1 EP_2, EP_3, and EP_4) in rat, the primer sets were designed as follows: 5′-GTACCCTGGCACTTGGTGTT-3′ (forward) and 5′-GTTC TCTCGGAAACGTCGAG-3′ (reverse) for EP_1, 5′-GTGCT GGTAACGGAACTGGT-3′ (forward) and 5′-CGTGGCCA GACTAAAGAAGG-3′ (reverse) for EP_2, 5′-CCAGCTTAT GGGGATCATGT-3′ (forward) and 5′-AACGGCGATTAGG AAGGAAT-3′ (reverse) for EP_3, and 5′-GGTGCAGAGAT CCAGATGGT-3′ (forward) and 5′-ATTCTGATGGCCTGC AAATC-3′ (reverse) for EP_4. PCR was performed using Taq DNA polymerase (Takara, Tokyo, Japan). The PCR cycling parameters consisted of 30 seconds denaturation at 94°C, 30 seconds annealing at 50°C, and 60 seconds extension at 72°C, for 35 cycles.

Real-time PCR for α-Skeletal Actin

In these experiments we used the EP_1 antagonist SC51322 (BIOMOL) and the EP_4 antagonist AE3-208 (kindly provided by Ono Pharmaceutical Co, Osaka, Japan). Cardiomyocytes were treated with PGE_2 (10 μM) alone for 24 hours or pretreated with SC51322 (10 μM) or AE3-208 (10 μM) for 1 hour and then treated with PGE_2 (10 μM) for 24 hours. The total RNA extraction from the cardiomyocytes and reverse transcription were performed as described above. The samples were analyzed for α-skeletal actin mRNA expression by real-time PCR. The primers were designed

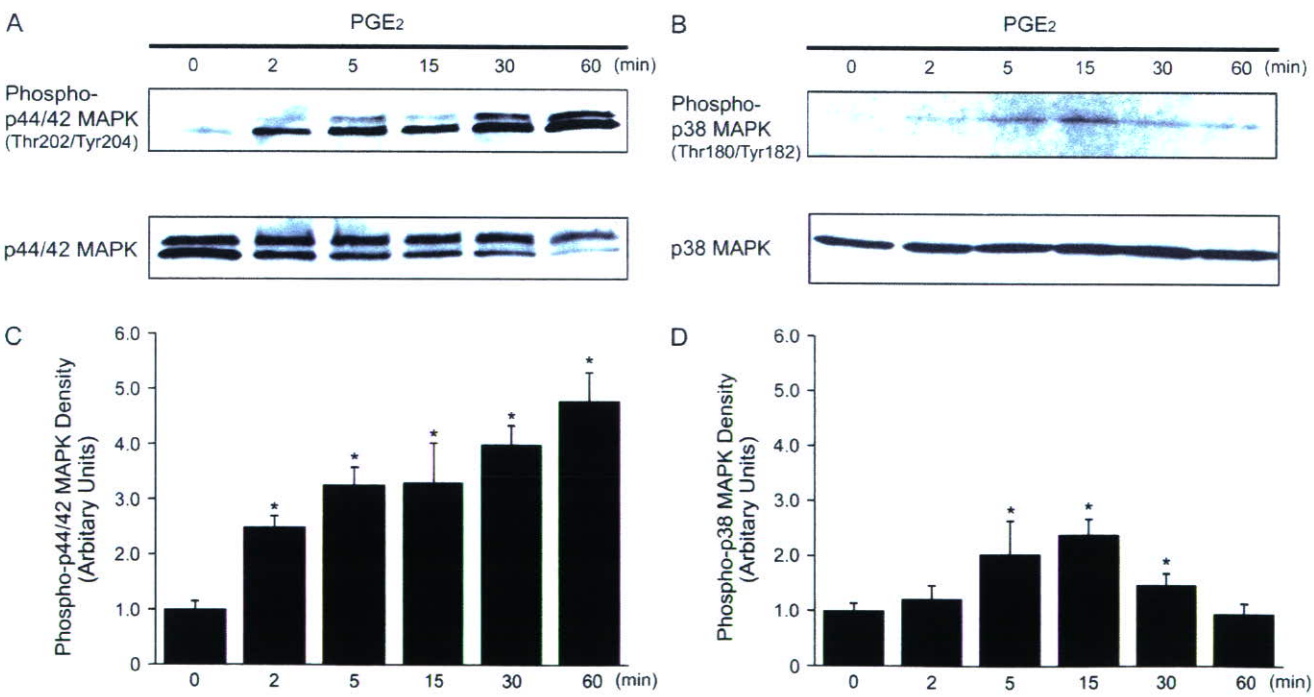

FIGURE 3. Effects of PGE_2 on phosphorylation of p42/44 MAPK and p38 MAPK in cardiomyocytes. Representative Western blot of phosphorylated p42/44 MAPK (Thr202/Tyr204) (A) and phosphorylated p38 MAPK (Thr180/Tyr182) (B) in cardiomyocytes stimulated with PGE_2 for the indicated times. Each lower panel shows the result of the reblotting against total p42/44 MAPK (A) and p38 MAPK (B), respectively. Densitometric analysis of the Western blot results is shown for phosphorylated p42/44 MAPK (C) and phosphorylated p38 MAPK (D). The results are normalized to the control values (0 minutes). Bars are the mean ± SD of 3 experiments. *$P < 0.05$ versus control.

from the 3′ untranslated region of the rat α-skeletal actin sequence (GenBank NM_019212), because this region is isotype specific.[28] The primers were 5′-CAGCCGGCGCCTGTT-3′ (forward), 5′-TCCACAGGGCTTTGTTTGAAA-3′ (reverse), and 5′-FAM-TTGACGTGTACATAGATTCACTCGTTTTACC TCATTTTG-TAMRA-3′ (probe). As an internal control, TaqMan rodent GAPDH control reagents (Applied Biosystems, Foster City, CA) were used. Real-time PCR was performed using an ABI 7500 Fast Real Time PCR System (Applied Biosystems), in accordance with the manufacturer's instructions. The expression of α-skeletal actin mRNA was normalized to that of GAPDH mRNA.

Statistical Analysis

All values are expressed as mean ± SD. The significance of differences between means was determined by ANOVA. Statistical comparison of the control group with the treated group was performed using Fisher multiple comparison tests. $P < 0.05$ was considered significant.

RESULTS

Effects of PGE_2 on [^{3}H]-Phenylalanine Uptake in Cardiomyocytes

Incubation of rat cardiomyocytes with PGE_2 increased the uptake of [^{3}H]-phenylalanine in a dose-dependent manner (Figure 1), indicating the stimulation of protein synthesis. The maximal increase occurred at a concentration of 250 μM and represented a 1.6-fold increase over the control.

Effects of PGE_2 on Myofibrillar Assembly and Cell Size in Cardiomyocytes

Stimulation with PGE_2 for 48 hours induced a striking rearrangement of myofibrillar assembly in cardiomyocytes, as shown by comparing immunofluorescence images of sarcomeric myosin in control and treated cardiomyocytes (Figure 2, A and B). Quantitative analyses revealed a 2.0-fold increase in cell surface area and a 1.5-fold increase in cell perimeter, compared to the control cells (Figure 2, C and D), indicating that PGE_2 also induced an enlargement of the cardiomyocytes.

PGE_2 Activated Phosphorylation of p42/44 MAPK and p38 MAPK in Cardiomyocytes

We next tested whether PGE_2 activated the p42/44 MPAK and p38 MAPK signaling pathways in cardiomyocytes. Western blot analyses revealed that PGE_2 phosphorylated both p42/44 MAPK and p38 MAPK in a time-dependent manner. In the presence of PGE_2, the phosphorylation of p42/44 MAPK (Thr202/Tyr204) increased from 2 minutes and reached a 4.8-fold increase over control at 60 minutes (Figure 3, A and C). PGE_2 also activated phosphorylation of p38 MAPK (Thr180/Tyr182), with a peak increase of 2.4-fold greater than control at 15 minutes, followed by a gradual decline (Figure 3, B and D). As shown by the densitometric analysis, the relative increase in phosphorylation of p42/44 MAPK induced by PGE_2 was markedly greater and more sustained than that of p38 MAPK. Western blot analysis using antibodies against total p42/44 MAPK and p38 MAPK indicated that PGE_2 did not alter the total expression of MAPK isoforms in the cardiomyocytes (Figure 3, A and B).

Role of p42/44 and p38 MAPK on PGE_2-induced Protein Synthesis

To investigate whether p42/44 and p38 MAPK were involved in PGE_2-induced protein synthesis, we preincubated U0126 (MEK1/2 inhibitor) or SB203580 (p38 MAPK inhibitor) and measured PGE_2-induced upregulation of [^{3}H]-phenylalanine uptake. U0126 significantly inhibited the PGE_2-induced [^{3}H]-phenylalanine uptake. SB203580 only slightly attenuated it, although the effect was statistically not significant (Figure 4).

PGE_2 Induced Expression of ANP and BNP mRNA, but Suppressed Expression of α-Skeletal Actin mRNA

To determine the effect of PGE_2 on hypertrophic marker genes such as ANP, BNP, and α-skeletal actin, we performed Northern blot analyses on PGE_2-stimulated cardiomyocytes. PGE_2 significantly augmented the expression of mRNA for both ANP and BNP (Figure 5, A and B). Densitometric analysis showed that the expression of mRNA for ANP increased 6.9-fold and that for BNP increased 2.1-fold compared to the control (Figure 5, D and E). Interestingly, however, PGE_2

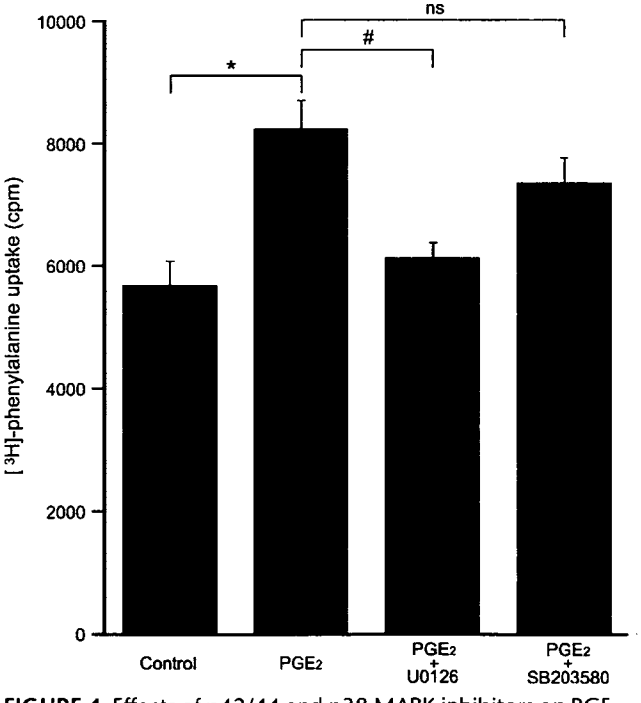

FIGURE 4. Effects of p42/44 and p38 MAPK inhibitors on PGE_2-induced [^{3}H]-phenylalanine uptake in cardiomyocytes. Cardiomyocytes were pretreated with U0126 (MEK 1/2 inhibitor) or SB203580 (p38 MAPK inhibitor) and then treated with PGE_2 for 24 hours. The measurement of [^{3}H]-phenylalanine uptake is indicated. Each column represents the mean ± SD of 4 separate experiments. *$P < 0.05$ versus control; #$P < 0.05$ versus PGE_2; ns, not significant versus PGE_2.

significantly attenuated the expression of mRNA for α-skeletal actin compared to the control cardiomyocytes (Figure 5C). The expression of mRNA for α-skeletal actin decreased to 27% of that in the control (Figure 5F).

PGE_2 Attenuated α-Skeletal Actin Gene Expression in Part via EP_4

To investigate which EP receptors are expressed in rat cardiomyocytes, we performed RT-PCR for the 4 EP receptors. mRNAs for all 4 EP receptors were detected in rat cardiomyocytes (Figure 6A). To investigate which EP receptors were involved in α-skeletal actin gene suppression, we used the receptor-specific antagonists, SC51322 and AE3-208, and performed real-time PCR for α-skeletal actin mRNA. SC51322 did not affect the PGE_2-induced attenuation of α-skeletal actin mRNA (Figure 6B), indicating that EP_1 was not involved. However, AE3-208 significantly inhibited the attenuation (Figure 6B), indicating that the action of PGE_2 was mediated at least in part by EP_4.

DISCUSSION

Cardiac hypertrophy is characterized by an increase in cell size and a number of qualitative and quantitative changes in gene expression. In this study, we showed that PGE_2 induced hypertrophic changes in primary cultured neonatal cardiomyocytes. PGE_2 increased [^{3}H]-phenylalanine uptake in a dose-dependent manner, produced an increase in cell size, and induced the reorganization of myofibrillar assemblies.

We demonstrated that PGE_2 induced phosphorylation of both p42/44 MAPK and p38 MAPK, though phosphorylation of p38 MAPK was minimal and its contribution on PGE_2-induced protein synthesis was statistically not significant. These results indicated that the activation of p42/44 MAPK might be critically involved in PGE_2-induced hypertrophic effect, and the contribution of p38 MAPK might be minimal in cardiomyocytes. The role of PGE_2-induced activation of p38 MAPK in cardiomyocytes remains uncertain. In other cells, PGE_2 regulates cyclooxygenase-2 (COX-2) mRNA stability through p38 MAPK, which suggests a positive feedback loop.[29] In cardiomyocytes, MAP kinase kinase 6 (MKK 6)-p38 MAPK signaling cascade is involved in regulation of COX-2 expression.[30] The role of p38 MAPK downstream of PGE_2 should be clarified in the future.

In this study, we demonstrated that PGE_2 augmented the expression of the hypertrophic marker genes, ANP and BNP, but significantly suppressed the expression of mRNA for α-skeletal actin. The gene for α-skeletal actin is activated by most cardiac hypertrophic stimuli, including other prostaglandin, prostaglandin $F_{2\alpha}$.[31] These stimuli activate the so-called fetal contractile pattern,[32] but several other stimuli such as IL-1β induce distinct hypertrophic phenotypes, in which the α-skeletal actin gene is not activated.[25] α-skeletal actin expression has been associated with increased contractility in the rodent heart,[33] while it also associated with impaired contractility in patients with dilated cardiomyopathy.[34,35] The linear correlation between an increase in α-skeletal actin expression and ventricular hypertrophy has been reported in

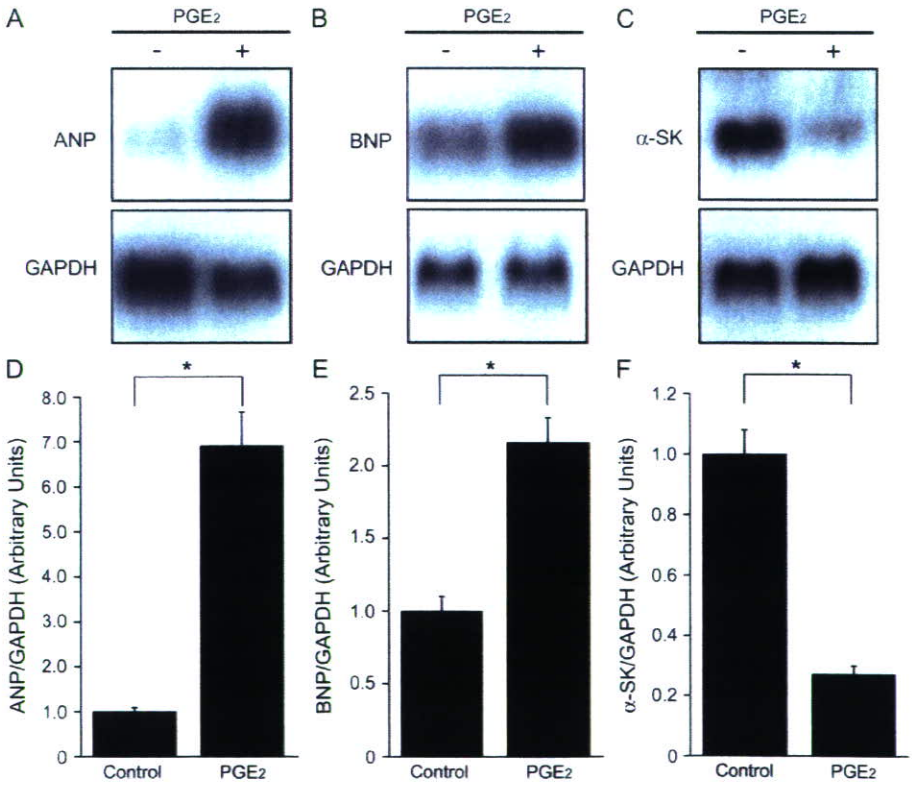

FIGURE 5. Effects of PGE_2 on hypertrophy marker genes expression in cardiomyocytes. Cardiomyocytes were incubated with or without PGE_2. Representative Northern blots are shown for ANP (A), BNP (B), and α-skeletal actin (α-SK) (C), Each lower panel shows equal loadings of GAPDH as an internal control. Densitometric analysis of the Northern blot results is shown for ANP (D), BNP (E), and α-skeletal actin (F) mRNA expression. Results are normalized to GAPDH mRNA levels and are expressed as fold increases relative to the control. Bars are the mean ± SD of 3 experiments. $^*P < 0.05$ versus control.

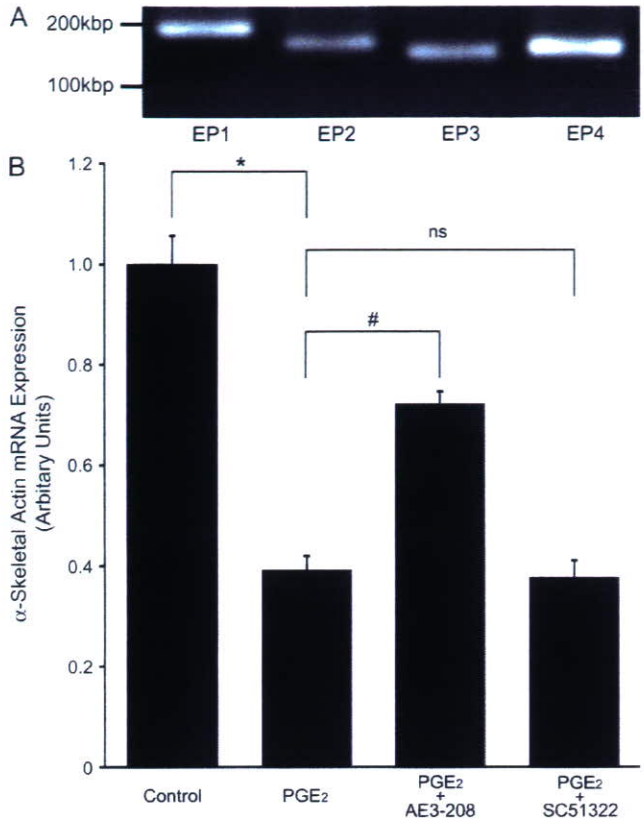

FIGURE 6. Effects of EP_1 and EP_4 antagonists on PGE_2-induced α-skeletal actin mRNA attenuation in cardiomyocytes. (A) RT-PCR showing the presence of mRNA for all 4 EP receptor subtypes in rat cardiomyocytes. (B) Real-time PCR analysis of α-skeletal actin mRNA expression. Cardiomyocytes were pretreated with SC51322 (EP_1-selective antagonist) or AE3-208 (EP_4-selective antagonist) and then treated with PGE_2. Results are normalized to GAPDH mRNA levels and are expressed as fold increases relative to the control. Bars represent the mean ± SD of 3 experiments. *$P < 0.05$ versus control; #$P < 0.05$ versus PGE_2; ns, not significant versus PGE_2.

the cardiac pressure overload model.[23] These findings may indicate that increase of α-skeletal actin expression in part acts as a compensatory mechanism. The significance of the PGE_2-induced suppression of α-skeletal actin remains unknown and needs to be clarified.

According to the mapping of α-skeletal actin promoter region, there are the motifs for the serum response factor (SRF), which binds to a serum response element (SRE), as well as Yin Yang-1 (YY1), Sp1, and transcriptional enhancer factor 1 (TEF-1).[36,37] Transcription of the α-skeletal actin gene appears to be regulated primarily by competition between YY1 and SRF for overlapping binding sites,[36,38,39] and YY-1 acts as a negative transcriptional regulator for the α-skeletal actin promoter.[36,40] IL-1β suppresses α-skeletal actin gene expression through the activation of YY-1 by both transcriptional and posttranscriptional mechanisms in cardiomyocytes.[41] PGE_2 and IL-1β induce a similar form of cardiac hypertrophy, given that both suppress α-skeletal actin gene expression.[40,41] Further study will be necessary to elucidate whether YY-1 is involved in the PGE_2-mediated α-skeletal actin gene suppression.

In this study, we demonstrated that mRNAs for all 4 EP receptors were present in neonatal rat cardiomyocytes. We also showed that an EP_4 antagonist substantially inhibited the PGE_2-induced suppression of α-skeletal actin gene expression, whereas an EP_1 antagonist did not. In cardiomyocytes, PGE_2 induces protein synthesis and activates the ANP and BNP promoter mainly via EP_4.[7,42] Our findings indicate that EP_4 is also involved in the PGE_2-induced suppression of the α-skeletal actin gene. However, the EP_4 antagonist did not completely abolish the PGE_2 effect, so other EP receptors may also play a part. The similarity and the difference among these 4 receptor subtypes on the phenotype of PGE_2-induced cardiac hypertrophy should be elucidated in the future.

CONCLUSION

PGE_2 induced hypertrophic changes in rat cardiomyocytes. Unlike many hypertrophic stimuli, PGE_2 attenuated expression of the α-skeletal actin gene. The effect on α-skeletal actin gene expression was mediated at least in part by EP_4.

REFERENCES

1. Funk CD. Prostaglandins and leukotrienes: advances in eicosanoid biology. *Science*. 2001;294:1871–1875.
2. Harris SG, Padilla J, Koumas L, et al. Prostaglandins as modulators of immunity. *Trends Immunol*. 2002;23:144–150.
3. Gupta RA, Dubois RN. Colorectal cancer prevention and treatment by inhibition of cyclooxygenase-2. *Nat Rev Cancer*. 2001;1:11–21.
4. Murakami M, Naraba H, Tanioka T, et al. Regulation of prostaglandin E_2 biosynthesis by inducible membrane-associated prostaglandin E_2 synthase that acts in concert with cyclooxygenase-2. *J Biol Chem*. 2000;275:32783–32792.
5. Narumiya S, Sugimoto Y, Ushikubi F. Prostanoid receptors: structures, properties, and functions. *Physiol Rev*. 1999;79:1193–1226.
6. Mendez M, LaPointe MC. Trophic effects of the cyclooxygenase-2 product prostaglandin E_2 in cardiac myocytes. *Hypertension*. 2002;39:382–388.
7. Mendez M, LaPointe MC. PGE_2-induced hypertrophy of cardiac myocytes involves EP_4 receptor-dependent activation of p42/44 MAPK and EGFR transactivation. *Am J Physiol Heart Circ Physiol*. 2005;288:H2111–H2117.
8. Jakobsson PJ, Thoren S, Morgenstern R, et al. Identification of human prostaglandin E synthase: a microsomal, glutathione-dependent, inducible enzyme, constituting a potential novel drug target. *Proc Natl Acad Sci USA*. 1999;96:7220–7225.
9. Watanabe K, Kurihara K, Tokunaga Y, et al. Two types of microsomal prostaglandin E synthase: glutathione-dependent and -independent prostaglandin E synthases. *Biochem Biophys Res Commun*. 1997;235:148–152.
10. Watanabe K, Kurihara K, Suzuki T. Purification and characterization of membrane-bound prostaglandin E synthase from bovine heart. *Biochim Biophys Acta*. 1999;1439:406–414.
11. Tanikawa N, Ohmiya Y, Ohkubo H, et al. Identification and characterization of a novel type of membrane-associated prostaglandin E synthase. *Biochem Biophys Res Commun*. 2002;291:884–889.
12. Tanioka T, Nakatani Y, Semmyo N, et al. Molecular identification of cytosolic prostaglandin E_2 synthase that is functionally coupled with cyclooxygenase-1 in immediate prostaglandin E_2 biosynthesis. *J Biol Chem*. 2000;275:32775–32782.
13. Giannico G, Mendez M, LaPointe MC. Regulation of the membrane-localized prostaglandin E synthases mPGES-1 and mPGES-2 in cardiac myocytes and fibroblasts. *Am J Physiol Heart Circ Physiol*. 2005;288:H165–H174.

14. Chien KR, Knowlton KU, Zhu H, et al. Regulation of cardiac gene expression during myocardial growth and hypertrophy: molecular studies of an adaptive physiologic response. *FASEB J.* 1991;5:3037–3046.
15. Nakagawa O, Ogawa Y, Itoh H, et al. Rapid transcriptional activation and early mRNA turnover of brain natriuretic peptide in cardiocyte hypertrophy. Evidence for brain natriuretic peptide as an "emergency" cardiac hormone against ventricular overload. *J Clin Invest.* 1995;96: 1280–1287.
16. Carrier L, Boheler KR, Chassagne C, et al. Expression of the sarcomeric actin isogenes in the rat heart with development and senescence. *Circ Res.* 1992;70:999–1005.
17. Sadoshima J, Izumo S. Molecular characterization of angiotensin II-induced hypertrophy of cardiac myocytes and hyperplasia of cardiac fibroblasts. Critical role of the AT1 receptor subtype. *Circ Res.* 1993;73: 413–423.
18. Martin XJ, Wynne DG, Glennon PE, et al. Regulation of expression of contractile proteins with cardiac hypertrophy and failure. *Mol Cell Biochem.* 1996;157:181–189.
19. Clement S, Pellieux C, Chaponnier C, et al. Angiotensin II stimulates alpha-skeletal actin expression in cadiomyocytes in vitro and in vivo in the absence of hypertension. *Differentiation.* 2001;69:66–74.
20. Ito H, Hirata Y, Hiroe M, et al. Endothelin-1 induces hypertrophy with enhanced expression of muscle-specific genes in cultured neonatal rat cardiomyocytes. *Circ Res.* 1991;69:209–15.
21. Schwartz K, de la Bastie D, Bouveret P, et al. Alpha-skeletal muscle actin mRNA's accumulate in hypertrophied adult rat hearts. *Circ Res.* 1986;59: 551–555.
22. Clement S, Chaponnier C, Gabbiani G. A subpopulation of cardiomyocytes expressing alpha-skeletal actin is identified by a specific polyclonal antibody. *Circ Res.* 1999;85:e51–e58.
23. Stilli D, Bocchi L, Berni R, et al. Correlation of alpha-skeletal actin expression, ventricular fibrosis and heart function with the degree of pressure overload cardiac hypertrophy in rats. *Exp Physiol.* 2006;91: 571–580.
24. Wollert KC, Taga T, Saito M, et al. Cardiotrophin-1 activates a distinct form of cardiac muscle cell hypertrophy. Assembly of sarcomeric units in series VIA gp130/leukemia inhibitory factor receptor-dependent pathways. *J Biol Chem.* 1996;271:9535–9545.
25. Palmer JN, Hartogensis WE, Patten M, et al. Interleukin-1 beta induces cardiac myocyte growth but inhibits cardiac fibroblast proliferation in culture. *J Clin Invest.* 1995;95:2555–2564.
26. Kodama H, Fukuda K, Pan J, et al. Leukemia inhibitory factor, a potent cardiac hypertrophic cytokine, activates the JAK/STAT pathway in rat cardiomyocytes. *Circ Res.* 1997;81:656–663.
27. Ito H, Hiroe M, Hirata Y, et al. Insulin-like growth factor-I induces hypertrophy with enhanced expression of muscle specific genes in cultured rat cardiomyocytes. *Circulation.* 1993;87:1715–1721.
28. Ponte P, Gunning P, Blau H, et al. Human actin genes are single copy for alpha-skeletal and alpha-cardiac actin but multicopy for beta- and gamma-cytoskeletal genes: 3′ untranslated regions are isotype specific but are conserved in evolution. *Mol Cell Biol.* 1983;3:1783–1791.
29. Faour WH, He Y, He QW, et al. Prostaglandin E_2 regulates the level and stability of cyclooxygenase-2 mRNA through activation of p38 mitogen-activated protein kinase in interleukin-1 beta-treated human synovial fibroblasts. *J Biol Chem.* 2001;276:31720–31731.
30. Degousee N, Martindale J, Stefanski E, et al. MAP kinase kinase 6-p38 MAP kinase signaling cascade regulates cyclooxygenase-2 expression in cardiac myocytes in vitro and in vivo. *Circ Res.* 2003;92:757–764.
31. Lai J, Jin H, Yang R, et al. Prostaglandin F_2 alpha induces cardiac myocyte hypertrophy in vitro and cardiac growth in vivo. *Am J Physiol.* 1996;271: H2197–H2208.
32. Schaub MC, Hefti MA, Harder BA, et al. Various hypertrophic stimuli induce distinct phenotypes in cardiomyocytes. *J Mol Med.* 1997;75: 901–920.
33. Hewett TE, Grupp IL, Grupp G, et al. Alpha-skeletal actin is associated with increased contractility in the mouse heart. *Circ Res.* 1994;74: 740–746.
34. Tanaka M, Hiroe M, Ito H, et al. Differential localization of atrial natriuretic peptide and skeletal alpha-actin messenger RNAs in left ventricular myocytes of patients with dilated cardiomyopathy. *J Am Coll Cardiol.* 1995;26:85–92.
35. Adachi S, Ito H, Tamamori M, et al. Skeletal and smooth muscle alpha-actin mRNA in endomyocardial biopsy samples of dilated cardiomyopathy patients. *Life Sci.* 1998;63:1779–91.
36. MacLellan WR, Lee TC, Schwartz RJ, et al. Transforming growth factor-beta response elements of the skeletal alpha-actin gene. Combinatorial action of serum response factor, YY1, and the SV40 enhancer-binding protein, TEF-1. *J Biol Chem.* 1994;269:16754–16760.
37. Lew AM, Glogauer M, McUlloch CA. Specific inhibition of skeletal alpha-actin gene transcription by applied mechanical forces through integrins and actin. *Biochem J.* 1999;341(Pt 3):647–653.
38. Lee TC, Chow KL, Fang P, et al. Activation of skeletal alpha-actin gene transcription: the cooperative formation of serum response factor-binding complexes over positive cis-acting promoter serum response elements displaces a negative-acting nuclear factor enriched in replicating myoblasts and nonmyogenic cells. *Mol Cell Biol.* 1991;11:5090–5100.
39. Gualberto A, LePage D, Pons G, et al. Functional antagonism between YY1 and the serum response factor. *Mol Cell Biol.* 1992;12:4209–4214.
40. Patten M, Hartogensis WE, Long CS. Interleukin-1beta is a negative transcriptional regulator of alpha1-adrenergic induced gene expression in cultured cardiac myocytes. *J Biol Chem.* 1996;271:21134–21141.
41. Patten M, Wang W, Aminololama-Shakeri S, et al. IL-1 beta increases abundance and activity of the negative transcriptional regulator yin yang-1 (YY1) in neonatal rat cardiac myocytes. *J Mol Cell Cardiol.* 2000;32: 1341–1352.
42. Qian JY, Leung A, Harding P, et al. PGE_2 stimulates human brain natriuretic peptide expression via EP_4 and p42/44 MAPK. *Am J Physiol Heart Circ Physiol.* 2006;290:H1740–H1746.

SHOCK
Injury, Inflammation, and Sepsis: Laboratory and Clinical Appro

ARTICLE LINKS:
PDF (476 K)

ADENOSINE TRIPHOSPHATE-SENSITIVE POTASSIUM CHANNELS PREVENT EXTENSION OF MYOCARDIAL ISCHEMIA TO SUBEPICARDIUM DURING HEMORRHAGIC SHOCK.

Original Article

Shock. POST ACCEPTANCE, 13 December 2007
*Nakagawa, Masahiro *; Hori, Shingo +; Adachi, Takeshi ++; Miyazaki, Koji *; Inoue, Soushin *; Suzuki, Masaru +; Mori, Hidezo [S]; Nakazawa, Hiroe [//]; Aikawa, Naoki +; Ogawa, Satoshi **

Abstract:
Cardiac dysfunction during hemorrhagic shock (HS) is associated with myocardial ischemia, during which adenosine triphosphate (ATP)-sensitive potassium (KATP) channels can be activated. We investigated the role of KATP channels in HS-induced myocardial ischemia. Canine HS was induced using an aortic reservoir to maintain the aortic pressure at a constant 40 mmHg. To visualize the myocardial ischemia as a nicotinamide adenine dinucleotide-fluorescent area, the beating hearts were rapidly cross-sectioned (120 ms) and freeze-clamped (-190[degrees]C) using a sampling device after 10 min of HS. The effect of a KATP channel blocker, glibenclamide (1 mg/kg, i.v.), on myocardial ischemia was also quantified. Regional myocardial blood flow was measured using heavy element-loaded nonradioactive microspheres. Myocardial ischemia developed in the subendocardium in the HS alone group, whereas it extended through all the cardiac layers in the glibenclamide-treatment group. The coadministration of a KATP channel opener, cromakalim (50 [mu]g/kg, i.v.), with glibenclamide prevented the extension of myocardial ischemia to the subepicardium. Glibenclamide decreased the myocardial ATP concentration selectively in the subepicardium during HS. The HS decreased myocardial blood flow transmurally, and after the administration of glibenclamide, further decreased the blood flow selectively in the subepicardium. These results suggest that KATP channels are activated during HS, enabling selective subepicardial coronary dilatation and protecting the myocardium from the extension of myocardial ischemia to the subepicardium.

meso-Tetrakis(α,α,α,α-*o*-amidophenyl)porphinatoiron(II) Bearing a Proximal Histidyl Group at the β-Pyrrolic Position via an Acyl Bond: Synthesis and O_2 Coordination in Aqueous Media

Akito Nakagawa,[1] Teruyuki Komatsu,*[1,2] and Eishun Tsuchida*[1]
[1]*Advanced Research Institute for Science and Engineering, Waseda University, 3-4-1 Okubo, Shinjuku-ku, Tokyo 169-8555*
[2]*PRESTO, Japan Science and Technology Agency (JST)*

(Received February 16, 2007; CL-070182; E-mail: teruyuki@waseda.jp, eishun@waseda.jp)

meso-Tetrakis(α,α,α,α-*o*-(1-methylcyclohexanamido)phenyl)porphinatoiron(III) bearing a proximal histidyl group at the β-pyrrolic position via an acyl bond (**4c**) has been synthesized. Human serum albumin (HSA) incorporating the ferrous complex (**4d**) formed a stable O_2 adduct under physiological conditions (pH 7.4, 37 °C). Although an electron-withdrawing acyl group is attached to the porphyrin periphery, the O_2-binding affinity of HSA-**4d** was slightly higher than that of a similar analogue with a histidyl–alkylene group (**2d**).

In the active centers of hemoproteins, a basic amino acid residue, axially coordinated to the prosthetic heme group, namely the proximal base, plays a crucial role in controlling their biological functions, for example, histidine in hemoglobin (Hb) and cysteine in cytochrome P450. To mimic the versatile performances of the hemoproteins, numerous porphyrin derivatives have been synthesized over the past decades.[1,2] The most important factor in the molecular design of these compounds is how to confer the proximal base into the porphyrin structure by a covalent bond.

We successfully introduced a histidyl–alkylene group to the β-pyrrolic position of *meso*-tetrakis(α,α,α,α-*o*-(1-methylcyclohexanamido)phenyl)porphine (**1a**) using the Vilsmeier reaction.[3] Human serum albumin (HSA) incorporating the ferrous complex (**2d**) can reversibly bind and release O_2 under physiological conditions (pH 7.4, 37 °C) in a fashion similar to Hb and myoglobin.[3b] The advantage of this strategy is to confer the proximal histidine to the porphyrin periphery in the last step of the synthesis.[3,4] However, the preparation processes are still labor-intensive: (1) formylation of the porphyrin, followed by (2) demetallation of copper, (3) reduction of –CHO to $-CH_2OH$, (4) connection with glutaric acid, and (5) binding of terminal histidine.[3,4] If the axial base can be introduced into the superstructured porphyrin in a few steps, it will lead to creating a new field in the hemoprotein model chemistry.

In this communication, we report for the first time, the one-step introduction of the 4-carboxybutanoyl group into the β-pyrrolic position of *meso*-tetrakis(α,α,α,α-*o*-(1-methylcyclohexanamido)phenyl)porphyrin, which is easily converted into the hisitidine-linked porphyrin (**4a**) by other two processes. The O_2-binding property of the HSA hybrid incorporating the ferrous complex (**4d**) was then investigated in aqueous media.

The copper(II) complex of the parent porphyrin (**1b**) was synthesized according to our previously reported procedure.[3] We have found that the 4-carboxybutanoyl group is introduced by the Friedel–Crafts reaction using glutaric anhydride and aluminium chloride ($AlCl_3$) (Scheme 1). The progress of the reaction was monitored by the red shift of the absorption maxima

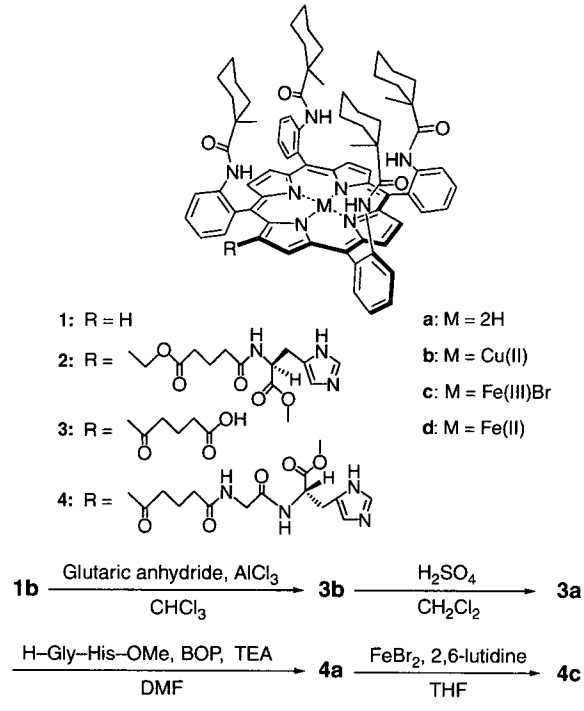

Scheme 1. Synthesis route of **4c**.

of the porphyrin and change in the R_f value during TLC. The brownish-red colored **3b** was purified by column chromatography and demetallated by H_2SO_4. The glycyl-*O*-methyl-L-histidine[5] was then coupled using benzotriazol-1-yl-oxytris(dimethylamino)phosphonium hexafluorophosphate (BOP). Finally, an iron insertion was carried out using $FeBr_2$ and 2,6-lutidine in anhydrous THF. The analytical data of all compounds described here were satisfactorily obtained (see Supporting Information).[6] The bathochromic shifts (3–7 nm) observed in the UV–vis absorption spectrum of **4a** compared to **2a** were due to the electron-withdrawing acyl group at the β-pyrrolic position.[6]

The ferric porphyrin (**4c**) in toluene was converted into the ferrous complex (**4d**) by reduction in a heterogeneous two-phase system (toluene/aq. $Na_2S_2O_4$) under an argon atmosphere.[4] The UV–vis absorption spectrum of the orange solution showed the formation of a five-N-coordinate high-spin complex (λ_{max}: 440, 544, 564 nm).[3,4,7] Upon exposure to O_2 or CO, the spectral pattern immediately changed to those of the O_2 adduct complex (λ_{max}: 429, 551 nm) or carbonyl complex (λ_{max}: 429, 544 nm).

The aqueous solution of the HSA-**4d** hybrid [in phosphate-buffered saline (PBS) solution (pH 7.4), [HSA]/[**4d**] = 1/4

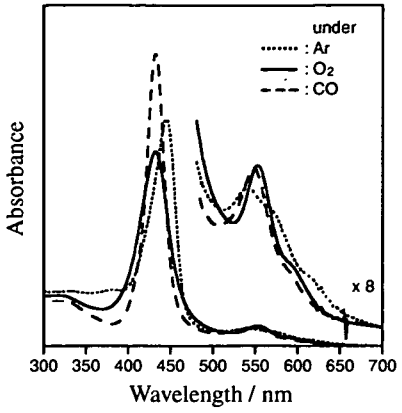

Figure 1. UV–vis absorption spectral changes of HSA-**4d** in PBS solution (pH 7.4) at 37 °C.

Table 1. O_2 binding parameters of HSA-porphinatoiron(II) in PBS solution (pH 7.4) at 25 °C[a]

Porphinatoiron(II)	$P_{1/2}$ /Torr	$k_{on}/\mu M^{-1} s^{-1}$		k_{off}/s^{-1}	
		fast	slow	fast	slow
2d[b]	1 (3)	54	8.8	89	14
4d	0.8 (2)	34	4.5	45	5.9

[a]The values in parenthesis are measured at 37 °C. [b]Ref 3b.

(mol/mol)] was prepared by a previously reported method.[3b] The UV–vis absorption spectrum of this aqueous solution under an argon atmosphere showed that **4d** formed a five-N-coordinate high-spin complex with an intramolecularly coordinated axial histidine (Figure 1). Upon exposure of HSA-**4d** to O_2, the absorption spectrum changed to that of the O_2 adduct complex. After reacting with the CO gas, a stable carbonyl complex was produced. The absorption maxima of HSA-**4d** showed 1–3 nm bathochromic shifts compared to those of the HSA-**2d** (Table S1).[3b,6]

The O_2-binding affinity of HSA-**4d** ($P_{1/2}$ = 0.8 Torr) determined by the spectral changes at the different O_2 partial pressures was slightly higher than that of HSA-**2d** (Table 1). This is in significant contrast to the fact that the substitutions of two 3,8-vinyl groups of the imidazole-bound protoporphinatoiron(II) by acetyl groups decreased the O_2-binding affinity by 1/4–1/6 due to the reduction of the electron density in the porphyrin plane.[8,9] Our result suggested that (1) the reduced basicity of the porphyrin core by the introduction of one acyl group did not influence the O_2-binding equilibrium very much, and (2) that there is another structural factor that increases the O_2-binding affinity of the porphyrin.

To determine the association and dissociation rate constants for O_2 (k_{on}, k_{off}) to HSA-**4d**, the laser flash photolysis experiments were carried out.[3b,10,11] The absorption decay accompanying the O_2 recombination was composed of two phases of first-order kinetics, producing the fast and slow rebinding constants [k_{on}(fast) and k_{on}(slow)]. The k_{on}(fast) value was 7.6-fold higher than k_{on}(slow), and the molar concentration ratio of the two reactions was 3:1. The O_2 association to **4d** in the protein scaffold might be influenced by the microenvironment around the coordination site. This behavior was similarly observed in HSA-**2d**.[3b] The characteristics of the O_2 binding to **4d** was kinetically the low k_{off} values (approximately 1/2) compared to **2d**.

The structures of the ferrous complexes were then simulated.[12] It is remarkable that the porphyrin plane of **2d** in the five-coordinate high-spin complex was significantly domed compared to that of **4d** (Figure S1).[6] On the other hand, their O_2 adduct complexes showed similar structures having the flat porphyrin macrocycles. The difference in the five-coordinate species could be caused by the spacer moiety between the histidine and porphyrin. The rigid (histidyl-glycyl)carbonylbutanoyl group of **4d** presumably produces a favorable geometry to fix the proximal imidazole at the central iron(II) of the porphyrin, which could result in the relatively low dissociation rate constant of O_2.

In conclusion, we could successfully introduce the proximal histidyl group at the β-pyrrolic position of the *meso*-(tetrakis-*o*-amidophenyl)porphine via an acyl bond in two steps. The O_2 binding affinity was slightly higher than that of the imidazolyl–alkylene analogue, which might be due to the rigid structure of the spacer moiety between the histidine and porphyrin ring. This strategy would be useful to confer the proximal base to the superstructured porphyrin without any change in the activity, which allows us to create a new class of model heme compounds.

This work was supported by a Grant-in-Aid for Young Scientists (B) (No. 18750156) and for Scientific Research (No. 16350093) from JSPS, PRESTO from JST, and Health Science Research Grants from MHLW, Japan.

References and Notes

1 M. Momenteau, C. A. Reed, *Chem. Rev.* **1994**, *94*, 659, and references therein.
2 a) J. P. Collman, L. Fu, *Acc. Chem. Res.* **1999**, *32*, 455. b) J. P. Collman, R. Boulatov, C. J. Sunderland, *Chem. Rev.* **2004**, *104*, 561.
3 a) T. Komatsu, Y. Matsukawa, K. Miyatake, E. Tsuchida, *Chem. Lett.* **2001**, 668. b) T. Komatsu, Y. Matsukawa, E. Tsuchida, *Bioconjugate Chem.* **2002**, *13*, 397.
4 E. Tsuchida, T. Komatsu, S. Kumamoto, K. Ando, H. Nishide, *J. Chem. Soc., Perkin Trans. 2* **1995**, 747.
5 E. Monzani, L. Linati, L. Casella, L. D. Gioia, M. Favretto, M. Gullotti, F. Chillemi, *Inorg. Chem. Acta* **1998**, *273*, 339.
6 Supporting Information is available electronically on the CSJ-Journal Web site, http://www.csj.jp/journals/chem-lett/index.html.
7 J. P. Collman, J. I. Brauman, T. J. Collins, B. L. Iverson, G. Lang, R. B. Pettman, J. L. Sessler, M. A. Walters, *J. Am. Chem. Soc.* **1983**, *105*, 3038.
8 A. Nakagawa, N. Ohmichi, T. Komatsu, E. Tsuchida, *Org. Biomol. Chem.* **2004**, *2*, 3108.
9 T. G. Traylor, D. K. White, D. H. Campbell, A. P. Berzinis, *J. Am. Chem. Soc.* **1981**, *103*, 4932.
10 J. P. Collman, J. I. Brauman, B. L. Iverson, J. L. Sessler, R. M. Morris, Q. H. Gibson, *J. Am. Chem. Soc.* **1983**, *105*, 3052.
11 T. G. Traylor, S. Tsuchiya, D. Campbell, M. Mitchell, D. Stynes, N. Koga, *J. Am. Chem. Soc.* **1985**, *107*, 604.
12 The esff forcefield simulation was performed using an Insight II system (Molecular Simulation Inc.). The structure was generated by alternative minimizations and annealing dynamic calculations from 1000 to 100 K.

Published on the web (Advance View) April 14, 2007; doi:10.1246/cl.2007.640

Influence of O_2-carrying plasma hemoprotein "albumin-heme" on complement system and platelet activation *in vitro* and physiological responses to exchange transfusion

Teruyuki Komatsu,[1] Yubin Huang,[1] Shinobu Wakamoto,[2] Hideki Abe,[2] Mitsuhiro Fujihara,[2] Hiroshi Azuma,[2] Hisami Ikeda,[2] Hisashi Yamamoto,[3,4] Hirohisa Horinouchi,[3] Koichi Kobayashi,[3] Eishun Tsuchida[1]

[1]*Advanced Research Institute for Science and Engineering, Waseda University, 3-4-1 Okubo, Shinjuku-ku, Tokyo 169-8555, Japan*

[2]*Research Department, Hokkaido Red Cross Blood Center, 2-2 Yamanote, Nishi-ku, Sapporo 063-0002, Japan*

[3]*Department of General Thoracic Surgery, School of Medicine, Keio University, 35 Shinanomachi, Shinjuku-ku, Tokyo 160-8582, Japan*

[4]*Pharmaceutical Research Center, NIPRO Corp., 3023 Noji-cho, Kusatsu-shi, Shiga 525-0055, Japan*

Received 23 March 2006; revised 13 July 2006; accepted 25 July 2006
Published online 18 January 2007 in Wiley InterScience (www.interscience.wiley.com). DOI: 10.1002/jbm.a.31016

Abstract: Recombinant human serum albumin (HSA) including the synthetic iron(II)-porphyrin (FeP), albumin-heme (HSA-FeP), is a unique O_2-carrying plasma hemoprotein as a red blood cell substitute. We have investigated the possible influence of HSA-FeP on the complement system and platelet activation *in vitro*. The amounts of the serum complement titer CH_{50} and terminal complement complex SC5b-9 of human blood serum, incubated with HSA-FeP (10, 20, and 40 vol %), were almost the same as those of the corresponding samples with HSA. The effect of HSA-FeP on the platelet reactivity has been demonstrated by conformational changes in the membrane glycoprotein IIb/IIIa and surface expression of an α-granule membrane protein P-selectin. Platelet activation in response to the ADP-stimulation was not influenced by the presence of HSA-FeP. It can be concluded that the albumin-heme solution does not facilitate the immunological reaction and platelet activation. Moreover, a 20% exchange transfusion with HSA-FeP into anesthetized rats has been performed to evaluate the circulation and blood parameters for 6 h. Time course changes in all parameters showed features identical to the control group (without infusion) and HSA group. © 2007 Wiley Periodicals, Inc. J Biomed Mater Res 81A: 821–826, 2007

Key words: albumin-heme; complement system; exchange transfusion; platelet activation; RBC substitute

INTRODUCTION

There has been significant progress in red blood cell (RBC) substitutes in the past decade, and several hemoglobin (Hb)-based products are currently in clinical II/III trials.[1–4] We have also developed a unique albumin-based O_2-carrier "albumin-heme," which is composed of recombinant human serum albumin (HSA) including synthetic heme (2-[8-{*N*-(2-methylimidazolyl)}-octanoyloxymethyl]-5,10,15,20-tetrakis(α,α,α,α-*o*-pivalamido)phenylporphinatoiron(II)) (FeP, Scheme 1) (HSA-FeP).[5–7] The HSA-FeP solution has a high compatibility with the blood cell components, and its O_2-transporting capability was evaluated by animal experiments.[8,9] Nevertheless, animal studies cannot predict the potential effect on human responses. Especially, immunological reactions and platelet activity need not be the same as those in animals. In this study, we report the possible influence of HSA-FeP on the human complement system and platelet activation *in vitro*.

It is known that the complement cascade is activated in trauma patients with or without hemorrhagic shock.[10] The large volume administration of HSA-FeP as a blood alternative to the human body may affect the total serum complement activity. We have measured the amounts of complement titer CH_{50} and the terminal complement complex SC5b-9 of the human blood serum after incubation with HSA-FeP.

On the other hand, the platelet activation process involves an ordered sequence of events. In particular, the

Correspondence to: E. Tsuchida; e-mail: eishun@waseda.jp
Contract grant sponsor: Health Science Research Grants, MHLW, Japan

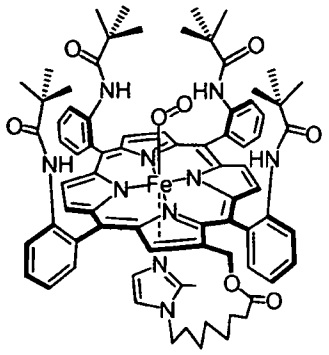

Scheme 1. Chemical structure of synthetic iron(II)-porphyrin (FeP) incorporated into HSA.

conformational changes in the membrane glycoprotein IIb/IIIa seem to be the most sensitive marker in the first event.[11–13] The activated GPIIb/IIIa creates a functional receptor for fibrinogen, which provides the link between adjacent platelets to form aggregates. The activation of this receptor can be detected by the specific monoclonal antibody PAC-1 that competes with fibrinogen.[11] The second event is the secretion of activation mediators, for example, ADP, serotonin, and thromboxane, resulting in further recruitment of platelets at the injured site.[14] The secretion process is accompanied by the rapid translocation of the α-granule membrane protein P-selectin (CD62P) to the outer membrane.[15,16] If the HSA-FeP solution activates the platelet, it may lead to amplifying the blood aggregation and inflammatory response. The PAC-1 binding and P-selectin surface expression have been assayed at the various levels of the ADP-stimulation.

Furthermore, we carried out the 20% exchange transfusion with the HSA-FeP solution into anesthetized rats and monitored the time courses of the circulation parameters (MAP, HR) and blood parameters (pH, PaO_2, PvO_2, $PaCO_2$) for 6 h.

MATERIALS AND METHODS

Materials

The recombinant human serum albumin (HSA, 25 wt %) was obtained from the NIPRO (Osaka). The HSA-FeP solution ([HSA]: 5.0 wt %, pH 7.4, [FeP]: 3.0 m*M*, COP: 21 mmHg, osmolarity: 300 mOsm, viscosity: 1.1 cP, endotoxin: <0.1 EU/mL, O_2-binding affinity ($P_{1/2}O_2$): 33 Torr) was prepared using our previously reported procedure.[8]

CH_{50} and SC5b-9

The human blood serum or plasma was well mixed with the HSA-FeP solution (the final concentration is 10, 20, and 40 vol %) and incubated for 1 h at 37°C. The CH_{50} value was determined by a 50% hemolysis assay based on Mayer's method with a commercial kit (New One point CH50 (KW), Japan BCG Supply, Tokyo). The SC5b-9 in the sample was determined using enzyme-linked immunosorbent assay kits (QUIDEL, Mountain View, CA).

PAC-1 and CD62P

The expression of PAC-1 and CD62P on platelets was measured as previously described.[17] Briefly, sodium citrate human whole blood was mixed with the HSA-FeP or HSA solution (the final concentration is 10, 20 and 40 vol %) and incubated for 10 min at 37°C. After adjusting the platelet concentration to

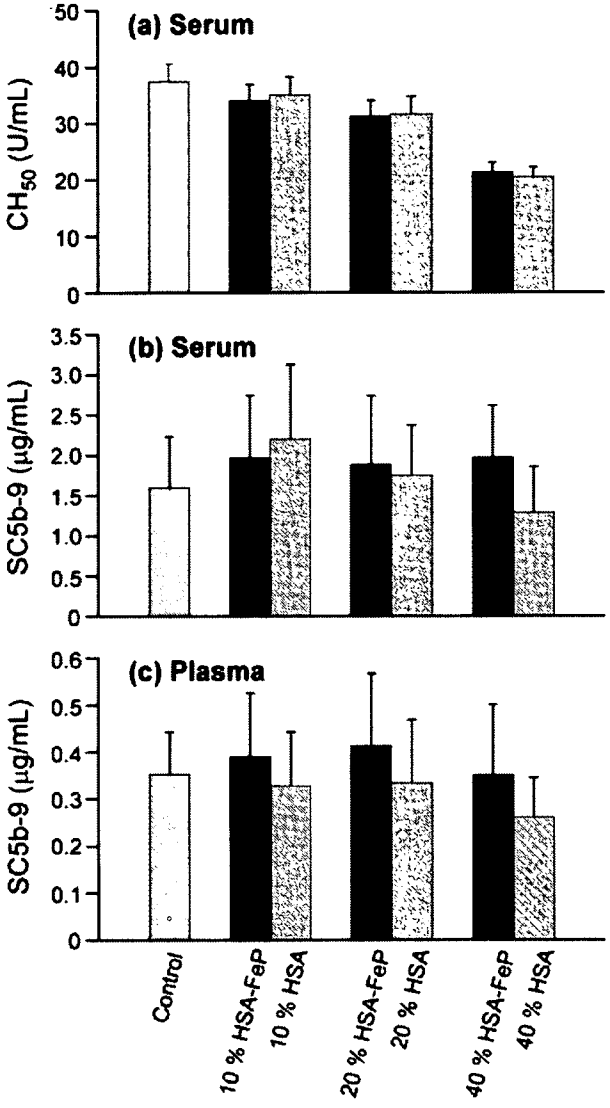

Figure 1. Influence of HSA-FeP on human serum complement after incubation for 1 h at 37°C; (a) serum complement titer (CH_{50}) in human blood serum, (b) terminal complement complex (SC5b-9) in human blood serum, and (c) SC5b-9 in human plasma. Each value represents the mean ± SD ($n = 5$).

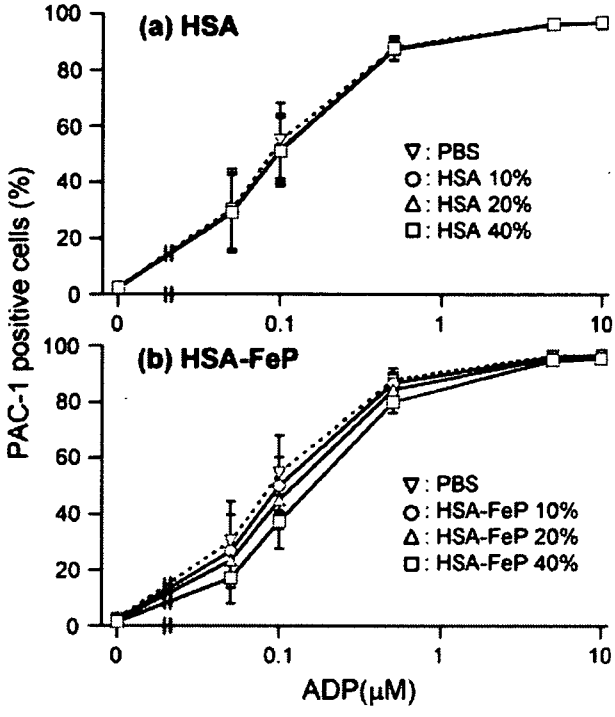

Figure 2. PAC-1 positive platelets in human whole blood mixed with (a) HSA-FeP and (b) HSA for 10 min at 37°C in response to various levels of ADP-stimulation. Each value represents the mean ± SD ($n = 5$).

$4 \times 10^5/20$ μL by Hepes Tyrode's buffer (pH 7.3), a cocktail of FITC-conjugated PAC-1, PE-conjugated anti-CD62P, and PerCP-conjugated anti-CD42a was added in equal amounts. A certain amount of ADP was added (the final ADP concentration is 0.05, 0.1, 0.5, 5, and 10 μ*M*). The FITC-conjugated anti-mouse IgM, PE-conjugated anti-mouse IgG, and PerCP-conjugated anti-mouse IgG were used as the negative controls. All antibodies were purchased from BD Bioscience-Pharmingen (San Jose, CA). The mixture was reacted in the dark for 20 min at room temperature and fixed with 1% paraformaldehyde. The samples were analyzed by flow cytometry (LSR, BD, San Jose, CA). Fluorescence data from 10,000 platelet events were collected in the logarithmic mode. The platelet population was identified by the number of CD42a positive events. The increased activation of GPIIb/IIIa and expression of CD62P were demonstrated by the percent of PAC-1 and CD62P positive cells in the platelets, respectively.

All subjects enrolled in this research had responded to an Informed Consent which has been approved by The Committee on Human Research of Hokkaido Red Cross, and that this protocol was found acceptable by them.

Exchange transfusion

The animal experiments using Wistar rats (304 ± 7.2 g) were carried out according to our previously reported protocol.[9] After stabilization of the animal, the 20% exchange transfusion was performed by 1 mL blood withdrawal via the common carotid artery and 1 mL HSA-FeP infusion from the femoral vein (each 1 mL/min); a total of four repeating cycles ($n = 6$, HSA-FeP group). A blood sample was taken from the artery (0.3 mL) and vein (0.2 mL) at the following five times; (1) before, (2) immediately after, (3) 1 h after, (4) 3 h after, and (5) 6 h after the exchange transfusion. MAP, HR, O_2-pressure (PaO_2), CO_2-pressure ($PaCO_2$) and pH for the arterial blood, and the O_2-pressure (PvO_2) of the venous blood were measured. As a reference group, the 5 g/dL HSA solution was similarly administered to the rats ($n = 6$, HSA group).[9] Furthermore, six rats without infusion (operation only) were also used as a control group.[9]

All animal handlings were in accordance with the NIH guidelines for the care and use of laboratory animals. The protocol details were approved by the Animal Care and Use Committee of Keio University.

Data analysis

All data were represented by mean ± standard deviation (SD). Statistical analyses were performed by repeated analysis measures of variance (ANOVA) using a StatView (SAS Institute). Values of $p < 0.05$ were considered significant.

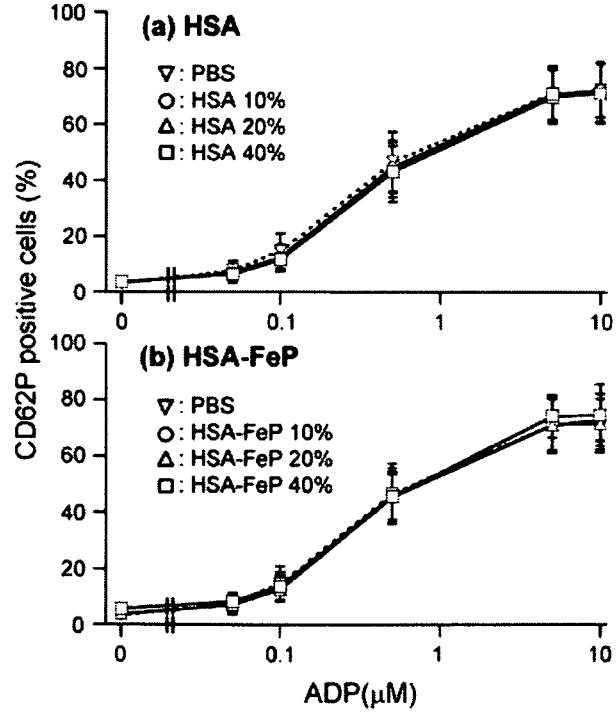

Figure 3. P-selectin expression on platelets in human whole blood mixed with (a) HSA-FeP and (b) HSA for 10 min at 37°C in response to various levels of ADP-stimulation. Each value represents the mean ± SD ($n = 5$).

RESULTS AND DISCUSSION

Complement system

Changes in the complement consumption are generally demonstrated by the complement titer CH_{50}. Ohtani et al. reported that the recombinant HSA, which is used for host albumin for HSA-FeP, shows the same immunochemical properties as the plasma HSA.[18] Thus the recombinant HSA should be a good reference in this experiment. The CH_{50} of the human blood serum incubated with 10, 20, and 40 vol % of the HSA-FeP solution were reasonably reduced in proportion to the each dilution ratio: 91, 83, and 57% of the control level [Fig. 1(a)]. The differences are almost the same as those observed in the HSA group, suggesting that the decrease in the CH_{50} with HSA-FeP did not involve any specific interaction.

On the other hand, the mean amounts of SC5b-9 in the human blood serum or plasma after the incubation with HSA-FeP were slightly higher than the control levels. However, all such differences were not significant within the experimental errors. Similar observations were found in the HSA group independent of the mixing ratio (10, 20, and 40 vol %). This implies that HSA-FeP does not enhance the production of SC5b-9.

Platelet activation

PAC-1 recognizes an epitope on the GPIIb/IIIa complex of activated platelets near the fibrinogen receptor.[19] We measured the percent of PAC-1 positive cells in the blood sample incubated with the HSA or HSA-FeP solution. When the ADP is absent, the fraction of the active cells was negligibly small, that is, 1.37–2.39%, independent of the mixing ratio of HSA or HSA-FeP (10, 20, and 40 vol %) (Fig. 2). The addition of a certain amount of ADP increased the PAC-1 positive cells, for instance, 96.9 % at 10 μM in the PBS group. It is rather remarkable that the coexistence of HSA and HSA-FeP (10–40 vol %) did not disturb this concentration dependence of the ADP-stimulation (Fig. 2).

The P-selectin (CD62P) on the activated platelet interacts with vascular endothelial cells to induce hemostasis. The percent of the P-selectin positive cells in the sample with HSA or HSA-FeP solution was 3.30–5.57% independent of the mixing ratio (10, 20, and 40 vol %) (Fig. 3). The addition of ADP enhances the numbers of active cells, and the concentration dependence curves observed in the HSA and HSA-FeP groups ([ADP] = 0.05–10 μM) were all identical to that of the PBS group. These results revealed that the platelet activation in response to the ADP-stimulation was not influenced by HSA-FeP. We concluded that albu-

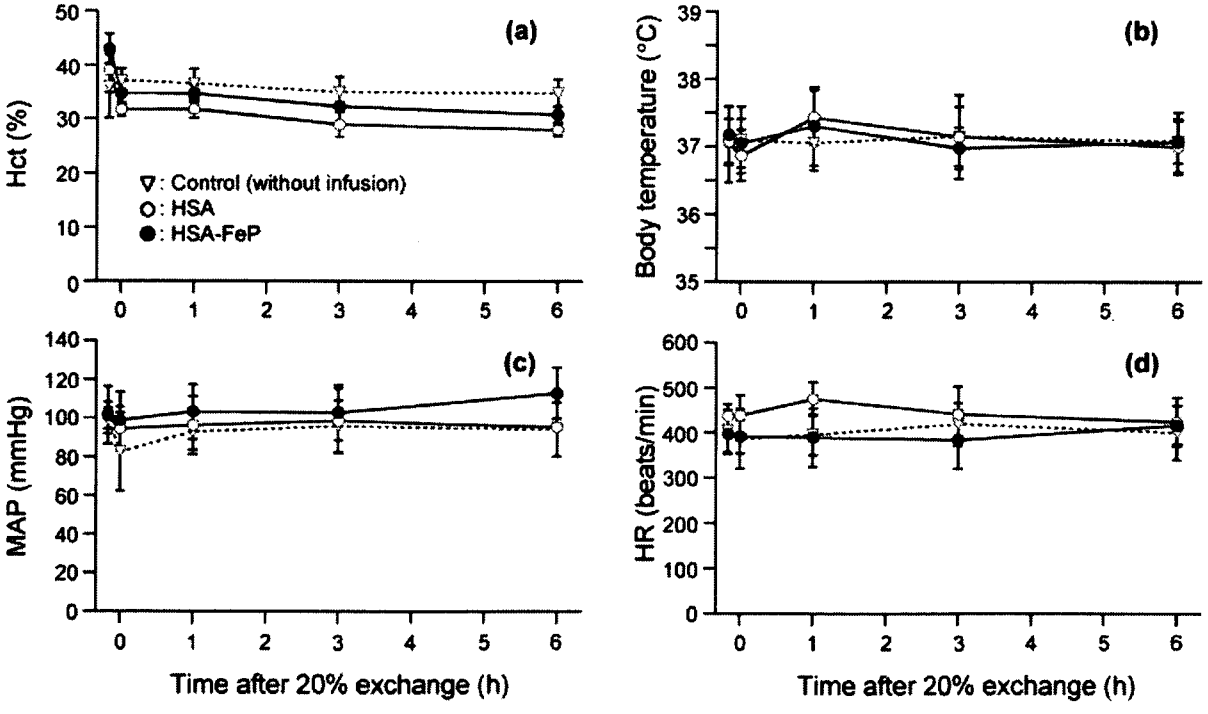

Figure 4. Time courses of (a) hematocrit (Hct), (b) body temperature, (c) mean arterial pressure (MAP), and (d) heart rate (HR) in anesthetized rats after 20% exchange transfusion with HSA-FeP or HSA solution. Each value represents the mean ± SD ($n = 6$).

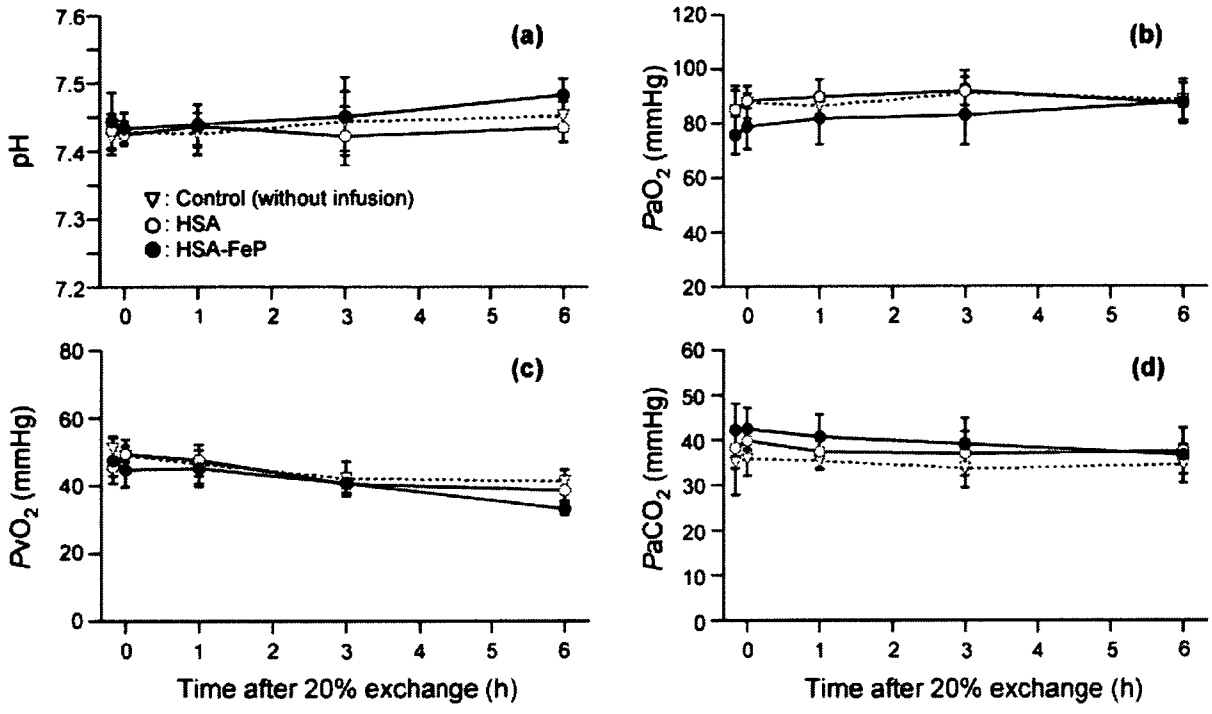

Figure 5. Time courses of (a) blood pH, (b) arterial blood O_2-pressure (PaO_2), (c) venous blood O_2-pressure (PvO_2), and (d) arterial blood CO_2-pressure ($PaCO_2$) in anesthetized rats after 20% exchange transfusion with HSA-FeP or HSA solution. Each value represents the mean ± SD ($n = 6$).

min-heme does not facilitate the immunological reaction and platelet activation in human blood at least based on the present test situation and degree.

Circulation parameters

After the 20% exchange transfusion with the HSA or HSA-FeP solution, Hct decreased ~80% of the basal values [Fig. 4(a)]. The body temperature of each group was maintained constant within 36.9–37.4°C during the experiments [Fig. 4(b)]. The time courses of MAP and HR of the HSA-FeP group were almost the same as those of the control or HSA group for 6 h [Fig. 4(c,d)]. Our previous studies showed that the infusion of HSA-FeP did not induce vasoconstriction and hypertension because of the low permeability of the albumin scaffold through the vascular endotheterlium.[20] It has been again demonstrated that absolutely no vasoactive response occurs after the 20% volume infusion of HSA-FeP.

Blood gas parameters

Changes in the blood gas parameters during the 20% exchange transfusion are shown in Figure 5(a–d). Differences in pH among the three groups were in the narrow range of 7.42–7.48 [Fig. 5(a)]. The PaO_2, PvO_2, and $PaCO_2$ values of the control, HSA, and HSA-FeP groups were also constant in the range of 78.9–91.8, 33.2–49.5, and 33.9–42.6 mmHg, respectively, by the end of the measurements [Fig. 5(b–d)]. These results revealed that HSA-FeP satisfies the initial preclinical safety as an RBC substitute.

In summary, one of the most prominent characteristics of the HSA-based O_2-carrier is its high blood compatibility, and no effect on the human immunological reaction and platelet activation. The appearance of the animals demonstrated no change for 6 h after the 20% exchange transfusion with HSA-FeP. The physiological responses in the HSA-FeP group were identical to those of the control and HSA groups. These results allow us to now undertake further advanced preclinical testing of this entirely synthetic O_2-carrier.

References

1. Chang TMS. Recent and future developments in modified hemoglobin and microencapsulated hemoglobin as red blood cell substitutes. Artif Cells Blood Substit Immobil Biotechnol 1997;25: 1–24.
2. Riess JG. Oxygen carriers ("blood substitute")—raison d'etre, chemistry, and some physiology. Chem Rev 2001;101:2797–2919.
3. Squires JE. Artificial blood. Science 2002;295:1002–1005.
4. Winslow R. Blood Substitutes. London: Elsevier; 2006.

5. Komatsu T, Hamamatsu K, Wu J, Tsuchida E. Physicochemical properties and O_2-coordination structure of human serum albumin incorporating tetrakis(*o*-pivamido)phenylporphyrinatoiron(II) derivatives. Bioconjug Chem 1999;10:82–86.
6. Tsuchida E, Komatsu T, Matsukawa Y, Hamamatsu K, Wu J. Human serum albumin incorporating tetrakis(*o*-pivalamido)-phenylporphinatoiron(II) derivative as a totally synthetic O_2-carrying hemoprotein. Bioconjug Chem 1999;10:797–802.
7. Komatsu T, Matsukawa Y, Tsuchida E. Effect of heme structure on O_2-binding properties of human serum albumin-heme hybrids: Intramolecular histidine coordination provides a stable O_2-adduct complex. Bioconjug Chem 2002;13:397–402.
8. Huang Y, Komatsu T, Nakagawa A, Tsuchida E, Kobayashi S. Compatibility in vitro of albumin-heme (O_2-carrier) with blood cell components. J Biomed Mater Res A 2003;66:292–297.
9. Hunag Y, Komatsu T, Yamamoto H, Horinouchi H, Kobayashi K, Tsuchida E. Exchange transfusion with entirely synthetic red-cell substitute albumin-heme into rats: Physiological responses and blood biochemical tests. J Biomed Mater Res A 2004;71:63–694.
10. Szebeni J, Wassef NM, Hartman KR, Alving CR. Complement activation in vitro by the red cell substitute, liposome-encapsulated hemoglobin: Mechanism of activation and inhibition by soluble complement receptor type 1. Transfusion 1997;37:150–159.
11. Shattil SJ, Hoxie A, Cunnington M, Brass LF. Changes in the platelet membrane glycoprotein IIb-IIIa complex during the platelet activation. J Biol Chem 1985;260:11107–11114.
12. Takagi J, Petre BM, Walz T, Springer TA. Global conformational rearrangements in integrin extracellular domains in outside-in and inside-out signaling. Cell 2002;110:599–611.
13. Xiao T, Takagi J, Coller BS, Wang JH, Springer TA. Structural basis for allostery in integrins and binding to fibrinogen-mimetic therapeutics. Nature 2004;432:59–67.
14. Marguerie GA, Plow EF, Edgington TS. Human platelets possess an inducible and saturable receptor specific for fibrinogen. J Biol Chem 1979;254:5357–5363.
15. Lasky LA. Selectin: Interpreters of cell-specific carbohydrate information during inflammation. Science 1992;258:964–969.
16. Stenberg PE, McEver RP, Shuman MA, Jacques YV, Bainton DF. A platelet alpha-granule membrane protein (GMP-140) is expressed on the plasma membrane after activation. J Cell Biol 1985;101:800–886.
17. Wakamoto S, Fujihara M, Abe H, Yamaguchi M, Azuma H, Ikeda H, Takeoka S, Tsuchida E. Effects of hemoglobin vesicles on resting and agonist-stimulated human platelets in vitro. Artif Cells Blood Substit Biotechnol 2005;33:101–111.
18. Ohtani W, Nawa Y, Takeshima K, Kamuro H, Kobayashi K, Ohmura T. Physiochemical and immunochemical properties of recombinant human serum albumin from *Pichia pastoris*. Anal Biochem 1998;256:56–62.
19. Taub R, Gould RJ, Garsky VM, Ciccarone TM, Hoxie J, Friedman PA, Shattil SJ. A monoclonal antibody against the platelet fibrinogen receptor contains a sequence that mimics a receptor recognition domain receptor. J Biol Chem 1989;264:259–265.
20. Tsuchida E, Komatsu T, Matsukawa Y, Nakagawa A, Sakai H, Kobayashi K, Suematsu M. Human serum albumin incorporating synthetic heme: Red blood cell substitute without hypertension by nitric oxide scavenging. J Biomed Mater Res A 2003;64:257–261.

Induced Long-Range Attractive Potentials of Human Serum Albumin by Ligand Binding

Takaaki Sato,[1,2,*] Teruyuki Komatsu,[2,3] Akito Nakagawa,[2] and Eishun Tsuchida[2,†]

[1]*Division of Pure and Applied Physics, Faculty of Science and Engineering, Waseda University, 3-4-1 Okubo, Shinjuku-ku, Tokyo 169-8555, Japan*

[2]*Advanced Research Institute for Science and Engineering, Waseda University, 3-4-1 Okubo, Shinjuku-ku, Tokyo 169-8555, Japan*

[3]*PRESTO, Japan Science and Technology Agency (JST), 4-1-8 Honcho, Kawaguchi-shi, Saitama 332-0012, Japan*

(Received 9 July 2006; published 15 May 2007)

Small-angle x-ray scattering and dielectric spectroscopy investigation on the solutions of recombinant human serum albumin and its heme hybrid revealed that heme incorporation induces a specific long-range attractive potential between protein molecules. This is evidenced by the enhanced forward intensity upon heme binding, despite no hindrance to rotatory Brownian motion, unbiased colloid osmotic pressure, and discontiguous nearest-neighbor distance, confirming monodispersity of the proteins. The heme-induced potential may play a trigger role in recognition of the ligand-filled human serum albumins in the circulatory system.

DOI: 10.1103/PhysRevLett.98.208101 PACS numbers: 87.14.Ee, 61.10.Eq, 83.80.Lz

Human serum albumin (HSA) is the most abundant plasma protein in our bloodstream, whose primary functions are transportation of hydrophobic molecules and adjustment of colloid osmotic pressure (COP) of blood [1]. Owing to its nonspecific ligand-binding capability, HSA has served many potential medical applications. Information on HSA-ligand interactions and their structural basis have recently been available by x-ray crystal structure analysis [2–5]. Such approaches have provided a structural foundation to create functional protein-ligand complexes. One of the promising materials is the rHSA-heme hybrid that can transport oxygen as hemoglobin does [6–9]. The material is currently investigated in preclinical tests as an artificial blood substitute [8]. Recent manifold interests in protein crystallography, critical phenomena, and disease processes have attracted increasing attention to interparticle interactions in globular protein solutions [10–15]. However, the fundamental problems like an influence of the ligand-binding upon protein-protein interactions remain elusive.

We investigated solutions of recombinant HSA (rHSA) (MW 66.5 kDa) and its heme hybrid [rHSA-heme; rHSA incorporating four iron-porphyrins (synthetic hemes)] [7]. Using small-angle x-ray scattering (SAXS), we scrutinized spatial correlations of these proteins in a 0.15M phosphate buffer saline (PBS) solution to fulfil ionic strength and pH close to physiological conditions and those in water to minimize ionic strength. The PBS solution of rHSA-heme (heme/rHSA = 4, mol/mol) was prepared according to our previously reported procedures [7]. The deionization of the protein sample was performed by several cycles of centrifugation/dilution with pure water using a Millipore Amicon Ultra to give aqueous solution of rHSA-heme. The solutions were passed through a 0.22 μm filter before all measurements. The deep red-colored, transparent solution of rHSA-heme can long be stored without precipitation or liquid-liquid phase separation. It has been confirmed that isoelectric point (pI), solution viscosity, and COP for rHSA-heme under the physiological environment are identical to those of rHSA.

All SAXS experiments were carried out by using a SAXSess camera (Anton Paar) in the q range of 0.072–5 nm^{-1}. A model-independent collimation-correction procedure was made via an indirect Fourier transformation (IFT) routine and/or based on a Lake algorithm. We also performed dielectric relaxation spectroscopy (DRS) experiments on aqueous rHSA and rHSA-heme solutions in the frequency range of $0.0005 \leq \nu/\mathrm{GHz} \leq 20$ using time domain reflectometry [16].

Figure 1 shows SAXS experiments on a concentration series of rHSA in PBS solution at 25 °C. The normalized scattered intensities $I(q)/c$, where $I(q)$ is the scattered intensity at scattering vector q and c the protein concentration, exhibit a decreasing forward intensity $I(q \to 0)/c$ with increasing c [Fig. 1(a)]. HSA carries a net negative charge of about 18 electronic charges at pH 7.4 [1]. Since the long-range electrostatic repulsion between rHSAs is efficiently screened in the PBS solutions, the suppressed forward intensity is mainly attributed to the decreased osmotic compressibility due to the increased particle number density. Lowering c results in the convergence of $I(q)/c$ to the intrinsic form factor $P(q)$ of rHSA, achieving the structure factor $S(q) \sim 1 (c \to 0)$.

The pair-distance distribution functions $p(r)$ of rHSA [Fig. 1(b)] in solution are obtained using generalized indirect Fourier transformation (GIFT) technique [17], for which we approximated $S(q)$ assuming a Yukawa potential and the Rogers-Young closure. The procedure confirms the existence of oblatelike particles having the maximum diameter of $D_{\max} \sim 8.0$–8.5 nm at all c. All features of $p(r)$ highly resemble those calculated from x-ray crystallography data on HSA (Protein Data Bank code 1UOR) [3].

Figure 2(a) presents variation of $I(q)$ of rHSA solutions, depending on the presence and absence of the heme incorporation and ionic strength of solvents. The more pronounced decrease of the forward intensity and the sig-

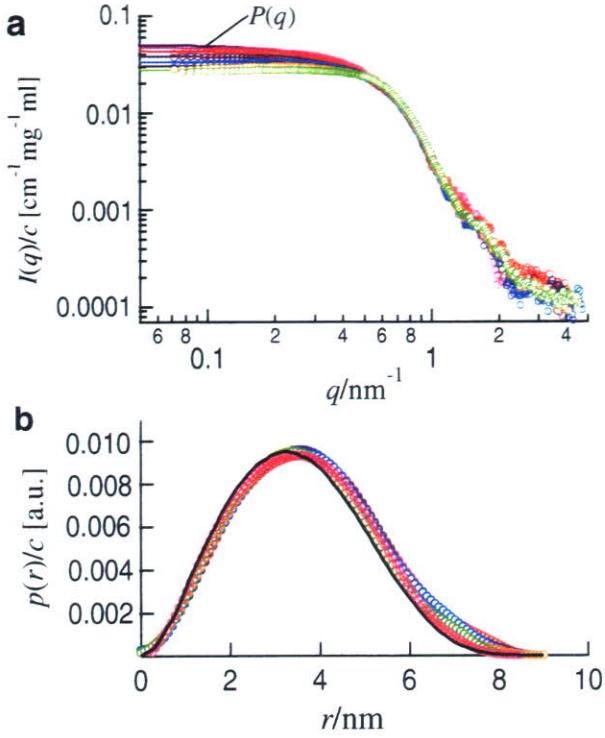

FIG. 1 (color online). (a) The normalized x-ray scattered intensities, $I(q)/c$, and (b) the pair-distance distribution functions, $p(r)$, of rHSA in 0.15M PBS solutions in $3.0 \leq c/\mathrm{mg\,ml^{-1}} \leq 50$. The black solid curve shown in (b) represents $p(r)$ calculated from the crystallography data on HSA [3].

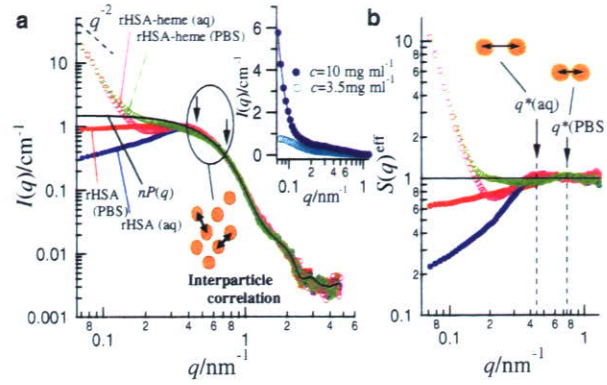

FIG. 2 (color online). (a) Variation of $I(q)$ and (b) the effective structure factors $S^{\mathrm{eff}}(q)$ for rHSA and rHSA-heme in aqueous and 0.15M PBS solutions of a fixed concentration $c = 30\ \mathrm{mg\,ml^{-1}}$. In the inset, the low-$q$ intensities for $c = 3.5\ \mathrm{mg\,ml^{-1}}$ and $c = 10\ \mathrm{mg\,ml^{-1}}$ are compared. Arrows on $S^{\mathrm{eff}}(q)$ highlight the monomer-monomer correlation peak positions q^*.

nificant low-q shift of the monomer-monomer correlation peak position for aqueous rHSA reflect the only weakly screened, thus stronger electrostatic repulsions between the rHSA molecules. Importantly, we observed that heme-incorporated samples exhibit an enhanced forward intensity, which indicates that heme incorporation significantly enhances particle density fluctuations on a large length scale.

Further insights into the spatial correlations between the proteins are gained from the effective structure factors $S^{\mathrm{eff}}(q)$ [11] [Fig. 2(b)]. We extracted $S^{\mathrm{eff}}(q)$ by dividing $I(q)/c$ by $P(q)$ obtained from a dilute rHSA PBS solution. We confirmed that for rHSA-heme, lowering c from 10 to 3.5 $\mathrm{mg\,ml^{-1}}$, leads to a significantly weaker relative low-q intensity, $I(q)/c$, as shown in Fig. 2. In terms of $S^{\mathrm{eff}}(q)$, rHSA under physiological condition still preserves the nature of a repulsively interacting charged colloid but behaves nearly as a hard sphere. If we apply a Yukawa potential model to $S^{\mathrm{eff}}(q)$ with *a priori* input of the solvent ionic strength, the effective protein charge of 18 ± 2 is obtained, being consistent with Ref. [1]. Solutions of rHSA-heme exhibit a similar low-q upturn in $S^{\mathrm{eff}}(q)$, independent of ionic strength. The observation suggests the emergence of a long-range attractive interaction [12,13] between the heme-incorporated rHSA molecules. However, this assignment is only valid when the monodispersity assumption of the protein is fulfilled. In the following, we carefully verify this interpretation, providing convincing evidence for monodispersity of rHSA-heme.

The peak in $S^{\mathrm{eff}}(q)$ arises from protein-protein positional correlations [Fig. 2(b)]. The mean nearest-neighbor distance d^* among the proteins is approximated as $\sim 2\pi/q^*$, where q^* is the scattering vector corresponding to the peak position of $S^{\mathrm{eff}}(q)$. Importantly, q^* is essentially independent before and after heme binding, but it simply depends on the solvent ionic strength related to the screening of the long-range electrostatic repulsion. In Fig. 3, we display a concentration series of $S^{\mathrm{eff}}(q)$ for rHSA and rHSA-heme solutions at different ionic strength. For aqueous rHSA and rHSA-heme, increasing c shifts q^* to higher values, holding a relation $q^* \propto n^{1/3}$ [Fig. 3(e)], where n is the particle number density. The finding clearly shows that both aqueous rHSA and rHSA-heme exhibit a typical feature of charged colloids at low ionic strength, maximizing d^*.

The identical COP (18 mmHg at $c = 50\ \mathrm{mg\,ml^{-1}}$) between the solutions of rHSA-heme and rHSA despite a half value for covalently dimerized rHSA at the same volume fraction [6] also rules out irreversible aggregate formation in rHSA-heme solutions. A simple model calculation demonstrates that a compact aggregate having several tens of aggregation number can never explain the observed low-q feature. No further enhancement of the low-q rise upon screening of the electrostatic repulsion excludes a strong short-range attraction as its origin.

Figure 4 presents complex dielectric spectra of rHSA and rHSA-heme solutions at various c. The relaxation time $\tau_{\mathrm{water}} \sim 8.3$ ps for the high-frequency process common for all solutions reflects the time scale of cooperative rearrangement of the hydrogen-bond network of bulk water [16,18,19]. Besides, the low-frequency relaxation, as-